



Published in final edited form as:

Neuron. 2019 July 17; 103(2): 277–291.e4. doi:10.1016/j.neuron.2019.04.037.

Rapid plasticity of higher-order thalamocortical inputs during sensory learning

Nicholas J. Audette^{1,2}, Sarah M. Bernhard¹, Ajit Ray¹, Luke T. Stewart¹, Alison L. Barth^{1,2,3,*}

¹Department of Biological Sciences, Carnegie Mellon University, Pittsburgh, PA, 15213, USA

²Center for the Neural Basis of Cognition, Carnegie Mellon University, Pittsburgh, PA, 15213, USA

³Lead Contact

Abstract

Neocortical circuits are sensitive to experience, showing both anatomical and electrophysiological changes in response to altered sensory input. We examined input- and cell-type specific changes in thalamo- and intracortical pathways during learning using an automated, home-cage sensory association training (SAT) paradigm coupling multi-whisker stimulation to a water reward. We found that POM, but not VPM, drives increased cortical activity after 24 hours of SAT, when behavioral evidence of learning first emerges. Synaptic strengthening within the POM thalamocortical pathway was first observed at thalamic inputs to L5 and was not generated by sensory stimulation alone. Synaptic changes in L2 were delayed relative to L5, requiring 48 hours of SAT to drive synaptic plasticity at thalamic and intracortical inputs onto L2 Pyr neurons. These data identify the POM thalamocortical circuit as a site of rapid synaptic plasticity during learning and suggest a temporal sequence to learning-evoked synaptic changes in the sensory cortex.

Introduction

Experience-dependent plasticity is a cardinal feature of the neocortex. Abundant evidence indicates that motor or perceptual learning drives changes in neocortical circuits, with changes observed in fMRI signals (Shibata et al., 2016; Summerfield et al., 2006), altered topographic organization (retino-, tono- or somatotopy; (Harris et al., 2001; Kilgard, 1998; Schwartz et al., 2002)), enhanced feature-selective responses and increased spike output to previously undetectable stimuli (Glazewski and Barth, 2015; Karni and Sagi, 1991), and increased synaptic strength (Cheetham et al., 2008; Clem, 2010; Rioult-Pedotti et al., 2000).

How is learning associated with plasticity in specific neocortical circuits? In rodent somatosensory cortex, experience-dependent changes are concentrated in infra- and

*Correspondence: albarth@andrew.cmu.edu.

Author Contributions

Conceptualization, N.J.A. and A.L.B.; Methodology, N.J.A., S.M. B., A.L.B.; Software, S.M.B.; Formal Analysis, N.J.A.; Investigation, N.J.A., L.T.S., A.R.; Writing – Original Draft, N.J.A., A.L.B.; Writing – Reviewing & Editing, N.J.A., S.B., L.T.S., A.R., A.L.B.; Visualization, N.J.A.; Supervision, A.L.B.; Funding Acquisition, N.J.A., A.R., A.L.B.

Declaration of Interests

The authors declare no competing interests.

supragranular layers, rather than layer 4 (L4 (Chandrasekaran et al., 2015; Diamond et al., 1994; Glazewski and Barth, 2015; Glazewski and Fox, 1996; Jacob et al., 2012; Oberlaender et al., 2012). This dissociation could be a product of post-synaptic differences, but also aligns with the laminar targets of the two thalamic input streams that drive the barrel cortex. The primary, ventral posterior-medial (VPM) thalamic nucleus provides the dominant glutamatergic input to L4 (Feldmeyer et al., 2013), while neurons in L2 and L5 receive strong glutamatergic input from the higher-order posterior-medial (POm) thalamic nucleus (Audette et al., 2017; Bureau et al., 2006; Petreanu et al., 2009), raising the possibility that the two thalamocortical circuits might be related to differences in plasticity induction across different cortical layers.

VPM neurons receive ascending sensory information directly from the trigeminal brain stem nucleus and respond robustly to the deflection of a single whisker (Feldmeyer et al., 2013). VPM faithfully relays these signals to L4 of the cortex, where excitatory neurons fire short-latency action potentials time-locked by fast, feedforward inhibition (Cruikshank et al., 2010; Feldmeyer et al., 2013). While VPM input plasticity has been observed in early development, electrophysiological and anatomical changes in L4 of the adult mouse are typically only detectable after prolonged periods of drastically altered sensory input levels (Crair and Malenka, 1995; Diamond et al., 1994; Fox, 1992; Glazewski and Fox, 1996; Oberlaender et al., 2012).

The higher-order thalamic nucleus POm also receives sensory signals from the brainstem, but integrates this information with strong cortical feedback from reciprocal connections to S1, S2, and M1 (Alloway et al., 2003; Groh et al., 2014; Urbain and Deschenes, 2007). Like other higher-order thalamic nuclei such as the pulvinar, POm neurons are well positioned to provide contextual information to the cortex and are strongly modulated by arousal and cholinergic activity (Masri et al., 2006; Purushothaman et al., 2012; Roth et al., 2016; Sobolewski et al., 2015). POm axon terminals, concentrated in L1 and L5, provide direct synaptic input to excitatory neurons in L2 and L5 (Audette et al., 2017; Bureau et al., 2006), and POm activation can prolong and enhance sensory responses in S1 (Mease et al., 2016). Plasticity of POm afferents onto L2 excitatory neurons can be elicited over short timescales by artificial whisker stimulation in anaesthetized mice, suggesting that these synapses possess the machinery for long-term potentiation (Gambino et al., 2014). Indeed, new findings indicate that POm activity in acute brain slices may facilitate intracortical plasticity through disinhibition (Williams and Holtmaat, 2019).

Since POm inputs can elicit activity-dependent synaptic strengthening, convey contextual and brain state information to the cortex, and drive activity in highly plastic cortical neuron populations, we hypothesized that POm-related pathways would undergo experience-dependent modifications during whisker-dependent learning. To test this, we developed a high-throughput, home-cage system for automated sensory association training that couples a multi-whisker stimulus to a water reward in freely-moving mice. Animals exhibit behavioral evidence of learning within the first 24 hours (hrs) of training, and performance increases with longer training intervals.

Using acute brain slices for pathway-specific activation and precise targeting of postsynaptic neurons across different cortical layers, we identified changes in excitatory synapses during early learning and then later, as behavioral performance improved. Neocortical responses to optogenetic activation of thalamic inputs were changed at the earliest stages of learning, where POM, but not VPM, drove significantly greater evoked firing in neocortical neurons in both deep and superficial layers after just 24 hrs of training. Synaptic strengthening of direct POM inputs to L5 neurons was linked to increased spiking during early training, but was not manifested in L2 neurons until 48 hrs of training. Evidence of synaptic strengthening in intracortical pathways, primarily at L2-L2 excitatory inputs, was delayed with respect to plasticity at POM synapses in L5. Importantly, these synaptic changes were not observed with unrewarded sensory stimulation. Together, our results indicate that plasticity at thalamic inputs from POM initiate cortical rewiring during sensory learning, revealing a temporal sequence of synaptic changes that begin in L5 and then progress to L2.

Results

Automated, home-cage sensory association training

Time-intensive animal training paradigms are not well-suited to a comprehensive electrophysiological analysis of cell-type and input-specific excitatory synaptic changes during learning. Thus, we designed an automated home-cage training system for freely-moving animals where a multi-whisker stimulus was predictively coupled to the cage water source (Figure 1A,B). We developed a mouse-initiated training paradigm adapted from classical trace conditioning, where a conditioned sensory stimulus (CS) was followed by an unconditioned stimulus (US) at a fixed delay (Galvez, 2006). A gentle airpuff was used as the CS, since it is a naturalistic stimulus and can activate multiple whiskers without precise animal positioning, well-suited for training freely-moving mice. On training trials, snout entry into the water port triggered a short random delay (200-800 ms) followed by a gentle airpuff (CS, 4-6 psi, 500 ms), a fixed delay (500 ms), and then water delivery (US, Figure 1B,D).

Blank trials, where no CS or US was delivered, were randomly interleaved on 20% of trials (Figure 1C,D). Prior to training, mice received one day of acclimation to the home-cage drinking setup where they experienced an identical trial structure but without presentation of the CS (Figure 1C). Mice readily learned to drink from the lick port and behavior data, including nose-poke times and licking, was recorded throughout the acclimation and training period.

In trace conditioning, the CS consistently predicts the US and becomes sufficient to evoke an unconditioned behavioral response, in this case licking (Cohen et al., 2012; Galvez, 2006). CS-US association was monitored by comparing the lick frequency prior to the time of potential water delivery, i.e. anticipatory licking (referred to as “licking”), between training and blank trials. Before sensory association training (SAT), licking was identical for both trial types (Figure 1E), as expected since no cue differentiated water-reward versus blank trials. A transient suppression of lick rates at the onset of SAT recovered rapidly, and the total trials/day were comparable between acclimation and training days (Figure 1G). By the end of the first day of training (24 hrs), mice increased their lick rate following the airpuff

but not on blank trials, evidence of a predictive CS-US association (Figure 1F-H)(Cohen et al., 2012).

Behavioral evidence of learning after 24 hrs of training was monitored by assessing the difference in licking for airpuff-water paired (L_{water} ; L_w) versus blank trials (L_{blank} ; L_b) over time to calculate a performance metric ($L_w - L_b$; Figure 1H). An increase in lick frequency for stimulus-paired trials was visible between 12 and 24 hrs and became significantly different from blank trials by 24 hrs. More than 75% of animals showed increased licking by the end of the first training day (Figure 1I). These data show that home-cage trace conditioning can drive the acquisition of a multi-whisker sensory association that is observable after just 24 hrs, which enabled electrophysiological investigation of circuitry changes at the earliest stages of sensory learning.

Increase in POM-evoked cortical activity after 24 hrs of SAT

To systematically evaluate the location of SAT-dependent modifications across the earliest stages of cortical processing in primary somatosensory cortex, we measured the response properties of cortical neurons following channelrhodopsin-assisted stimulation of the primary sensory thalamic nucleus, VPM or the higher-order nucleus POM, in acute brain slices. We examined how POM-evoked firing was changed by SAT by recording from pyramidal neurons (Pyr) in the major POM-recipient layers, L2 and L5 (Audette et al., 2017; Bureau et al., 2006; Viaene et al., 2011) after activation of thalamic axons. To isolate cortical responses specific to this pathway, ChR2 was expressed in POM (Figure S1). Although virally-expressed ChR2 expression can vary across animals, strict criteria were used to ensure a minimum level of ChR2 viral transduction monitored by fluorescence signal in cortical POM afferents. Animals were assigned to control or SAT groups without prior knowledge of ChR2 expression levels and average fluorescent labeling was comparable across groups.

In tissue from control animals (acclimation but no whisker stimuli), optogenetic stimulation of POM axons (5 pulses, 80ms ISI) drove short latency spiking in L5 Pyr (14.6 ± 3.4 ms; Figure S1) and subthreshold excitatory post-synaptic potentials (EPSPs) in L2 Pyr, consistent with prior work (Figure 2C, H)(Audette et al., 2017). POM stimulation occasionally caused prolonged, recurrent sub- and suprathreshold activity in the post-stimulus period that lasted for several seconds, although action potentials were only rarely observed in L2. Both spike probability and EPSP amplitude depressed with subsequent stimuli in L5 Pyr (Figure 2H,K; Figure S1)(Audette et al., 2017).

After 24 hrs of SAT, POM-evoked cortical firing was dramatically increased (Figure 2D,I). The fraction of neurons spiking during the stimulus and/or the post-stimulus period increased from 60% to 92% in L5, and 14% to 63% in L2. In L5, the SAT-associated change in POM spiking was most notable in response to the first light pulse, where mean firing frequency in the first 10ms after POM stimulation increased 4-fold (control 1.65 ± 1.0 Hz; 24 hrs SAT 4.25 ± 1.3 Hz), and the latency to spike was slightly reduced (control 14.6 ± 3.4 ms; 24 hrs SAT 13 ± 3.2 ms; Figure S1). L2 Pyr spiking during the 500 ms stimulus window increased nearly 20-fold (control 0.02 ± 0.02 Hz; 24 hrs SAT 0.33 ± 0.2 Hz), with the majority of spike output occurring later in the stimulus train. Spikes in L2 Pyr neurons typically

occurred 10-40 ms after an individual light pulse stimulus and showed high trial-to-trial variability (Figure S1). Where whole cell recordings were performed, we calculated the subthreshold EPSP amplitude evoked by stimulation of POM inputs to the barrel cortex. Overall, EPSPs evoked by the first light pulse in the stimulus train were similar for control and SAT24 animals in L2 (control 4.24 ± 0.87 mV $n=11$ cells; 24 hrs SAT 4.36 ± 0.71 mV $n=18$ cells), while EPSPs increased modestly in L5 after training (control 7.14 ± 1.6 mV $n=6$ cells; 24 hrs SAT 8.27 ± 1.4 mV $n=4$ cells). However, these values are difficult to interpret as the EPSP peak amplitude under these recording conditions likely represents a composite of thalamic and local polysynaptic input driven by strong ChR2 activation. Additionally, cells that consistently fired POM-evoked action potentials had to be excluded from PSP measurements since the presence of a spike made accurate detection of PSP amplitude impossible. Because L5 neurons were more likely to spike with POM activation after SAT, this dataset was particularly affected (8/12 cells fired with POM stimulation and were excluded from analysis).

In trained mice, POM stimulation evoked markedly increased levels of prolonged depolarization during the post-stimulus period for neurons in both L2 and L5 apparent in both firing rate (L2 control 0.02 ± 0.02 Hz; L2 24 hrs SAT 0.13 ± 0.04 Hz; L5 control 0.15 ± 0.11 Hz; L5 24 hrs SAT 0.76 ± 0.26 Hz; Figure 2E,J) and peak subthreshold activity in the 1s period following the stimulus train (L2 control 2.39 ± 0.48 mV $n = 11$ cells; L2 24 hrs SAT 5.20 ± 0.68 mV $n = 18$ cells; L5 control 1.86 ± 0.72 mV $n = 6$ cells; L5 24 hrs SAT 2.79 ± 0.65 mV $n = 6$ cells). These results indicate that 24 hrs of SAT drives a marked increase in Pyr responses to POM stimulation that are manifested across the cortical column.

VPM-evoked responses are unchanged

Although plasticity at VPM inputs is generally restricted to early development in L4, VPM axon remodeling in L4 has been observed in adult animals (Oberlaender et al., 2012), and VPM-related plasticity in other cortical layers has not been well-investigated. We used optogenetic activation of ChR2-expressing VPM afferents to screen for changes in evoked firing of regular spiking (L4) or Pyr neurons in L2 and L5, which receive both direct and indirect VPM input.

We first investigated SAT-induced changes in L4, the main VPM-recipient layer (Bureau et al., 2006; Cruikshank et al., 2010; Meyer et al., 2010). In control animals, optogenetic stimulation of VPM axons drove precisely timed, short-latency (10.1 ± 1.5 ms) action potentials in the majority (55%) of L4 neurons that were restricted to the stimulus window (Figure 3H,I) (Cruikshank et al., 2010). After SAT, a slightly smaller fraction of L4 neurons fired with VPM stimulation (43%), and spike latencies were unchanged (Figure S2G,H). The mean firing frequency across the entire stimulus period was indistinguishable between control and SAT (control 2.89 ± 0.98 Hz; 24 hrs SAT 2.58 ± 0.86 Hz, Figure 3J) and subthreshold EPSP amplitude remained unchanged (control 10.18 ± 1.48 mV $n = 12$ cells; 24 hrs SAT 9.59 ± 1.18 mV $n = 9$ cells). Unlike POM-evoked activity in L2 and L5, VPM stimulation never drove recurrent firing in the post-stimulus period, consistent with strong feed-forward inhibition in this layer (Cruikshank et al., 2010; Porter et al., 2001).

VPM provides direct synaptic input to L5 (Bureau et al., 2006; Meyer et al., 2010), and SAT could conceivably drive changes at this connection. Indeed, experience-dependent changes in L5 firing have been observed in some studies (Diamond et al., 1994; Jacob et al., 2012; Ward et al., 2012a), and the change in POM-evoked firing in L5 we observed might reflect a special capacity for plasticity of neurons in this layer. However, optogenetic activation of VPM afferents revealed that SAT did not change the fraction of L5 spiking neurons (50% for both conditions) or their mean evoked firing frequency during or after the stimulus window (Figure 3L-P). Thus, the pathway-specific activation of thalamic afferents in acute brain slices reveals an input-dependent, SAT-induced change in L5 response properties, something that would not have been easy to decipher from sensory stimulation *in vivo*.

L2 Pyr neurons receive minimal direct input from VPM, but do receive strong ascending input from L4. Consistent with this circuitry, optogenetic activation of VPM afferents in control samples was sufficient to drive firing in a fraction of L2 Pyr neurons (38%) that was delayed compared to spikes generated in deeper layers (L2 24.3 ± 0.5 ms; L4 10.1 ± 1.5 ms; L5 14.0 ± 1.7 ms; Figure S2). SAT did not change the fraction of spiking neurons (33%) or the mean evoked firing response during the stimulus period. As in L4, VPM stimulation did not elicit prolonged depolarization in the post-stimulus window for either L2 or L5 (Figure 3E,O).

Lack of changes in VPM-evoked firing could result from a homeostatic reduction in intrinsic excitability (Lambo and Turrigiano, 2013; Mrsic-Flogel et al., 2007). However, input-output curves and resting membrane potential for L2, L4, and L5 excitatory neurons showed no significant increase in either property between control and SAT neurons (Figure 4).

Our assay indicates that VPM-associated cortical pathways do not become potentiated during learning. Although L4 to L2/3 synapses can undergo spike-timing dependent plasticity (STDP) *in vitro* (Banerjee et al., 2009), the conditions engaged by SAT *in vivo* may not be sufficient to activate these well-described mechanisms. These results point to a special role for POM during learning-related changes in cortical response properties.

Target-specific potentiation of POM inputs

The increase in POM-evoked firing in both supra- and infragranular layers following 24 hrs of SAT, despite unchanged intrinsic firing properties, suggested that POM inputs to Pyr neurons might be strengthened after SAT. To compare the amplitude of quantal excitatory postsynaptic currents (qEPSCs) directly evoked from POM, we carried out voltage-clamp recordings from Pyr neurons during ChR2-activation of POM afferents in the presence of Sr^{++} to desynchronize neurotransmitter release. This method enables detection of EPSCs from individual synapses and can provide evidence for postsynaptic plasticity (Clem and Barth, 2006).

The short latency of POM-evoked spikes in L5 Pyr, both in control and SAT neurons, suggested that these L5 neurons were firing as a direct result of POM input. Thus, we hypothesized that POM inputs to L5 Pyr might be potentiated. After 24 hrs of SAT, the mean amplitude of POM-mediated qEPSCs was significantly increased (control 15.7 ± 0.5 pA; 24 hrs SAT 20.7 ± 0.6 pA; Figure 5F-H) and the cumulative distribution of qEPSC amplitudes

showed a rightward shift (Figure 5H). Consistent with other studies where experience has driven pathway-specific excitatory strengthening (Biane et al., 2016; Clem and Barth, 2006), we also observed a significant increase in the ratio of ChR2-evoked AMPA receptor: NMDA receptor-mediated currents (A:N ratio, control 1.89 ± 0.13 ; 24 hrs SAT 2.84 ± 0.29 ; $p=0.027$; Figure S3A-C). Although changes in presynaptic release properties are difficult to accurately assess with ChR2-evoked release, we examined our data for training-induced changes in the paired-pulse ratio (PPR) and found it unchanged at 24 hrs of SAT (control 0.39 ± 0.04 ; 24 hrs SAT 0.41 ± 0.06 ; Figure S3D-F).

Although POM recipient L2 Pyr neurons also exhibited an increase in evoked firing after 24 hrs SAT, mean POM-qEPSC amplitudes were unchanged between control and SAT neurons (control 17.8 ± 0.8 pA; 24 hrs SAT 18.3 ± 0.8 pA; Figure 5B-D). Significant differences were not observed even in the cumulative distribution of qEPSCs, suggesting that this pathway is unaltered at this time point in learning (Figure 5D).

Synaptic strengthening at POM to L5 synapses may be well positioned to facilitate further changes in neocortical circuitry, since these neurons show short spike latencies in response to POM stimulation and increase their POM-evoked firing after SAT (Figure 2 and Figure S1). The lack of even modest potentiation at POM to L2 synapses at this time point suggests that the conditions for the induction of synaptic plasticity are different between L2 and L5 Pyr neurons, in the behaving animal.

Elevated POM-evoked activity is driven by ascending input from infragranular layers

SAT increases POM-evoked firing of L2 Pyr neurons both during and after the optogenetic stimulus window. If POM inputs to L2 are not potentiated after 24 hrs of SAT, we hypothesized that this increased activity may be inherited from spiking in other cortical layers. For example, POM-evoked spikes in L5 occur within 15 ms of the optogenetic pulse, and ascending input from L5 Pyr to L2 could summate with direct POM EPSPs in L2 neurons to drive firing in these neurons. Indeed, POM-evoked EPSPs in L2 Pyr neurons were often complex, where individual trials showed multiple inflection points during the EPSP rise time that correspond to asynchronous synaptic inputs (Figure 6).

Thus, we hypothesized that POM-initiated, delayed synaptic input from deeper layers could contribute to the polysynaptic EPSPs and spiking activity observed in L2 Pyr. To test this, we compared the POM-evoked response properties of L2 Pyr neurons, before and after mechanical separation of supra- and infragranular layers, in acute brain slices from mice trained for 24 hrs (Figure 6A-D). Neurons were paired from the same region of the same slice before and after transection to ensure the initial presence of POM-evoked activity. The incision through L4 should not affect light-evoked neurotransmitter release, since channelrhodopsin can drive vesicle release directly by illumination of the synaptic terminal.

Slice transection completely abolished POM-evoked action potentials in L2 Pyr neurons (Figure 6D,G), without changing resting membrane potential (control -66.7 ± 1.9 mV; 24 hrs SAT -69.0 ± 1.9 mV). EPSP onset latency and slope were not altered (onset latency: control 4.6 ± 0.3 ms; 24 hrs SAT 5.0 ± 0.6 ms; slope: control 0.37 ± 0.06 ; 24 hrs SAT 0.35 ± 0.09), but

EPSP peak latency was significantly shorter (control 38.3 ± 3.8 ms; 24 hrs SAT 26.9 ± 1.5 ms), consistent with the loss of polysynaptic input originating in infragranular layers. After slice transection, POm stimulation no longer initiated prolonged depolarization in L2, indicating that POm-driven activity from deeper layers is also important in initiating or maintaining activity in the post-stimulus window. These data indicate that the increase in POm-evoked L2 firing relies upon convergent excitation from both POm and infragranular layers.

Intracortical changes are not present at 24 hrs of training

The increase in L2 POm-evoked firing after 24 hrs of SAT could result solely from the increase in synaptic drive from POm to L5 that is inherited by L2 Pyr, or could occur concurrently with excitatory synaptic potentiation within L5 or at L5 inputs to L2 Pyr. We examined both pathways using Sr^{++} -replaced ACSF to isolate pathway-specific quantal EPSCs.

To examine SAT-associated changes within the L5 local excitatory circuit, we used an extracellular stimulating electrode placed in L5 and recorded quantal EPSCs in L5 Pyr neurons (Figure S4). Although this method cannot isolate inputs from specific types of presynaptic neurons, the dense local connectivity within a cortical layer (Lefort et al., 2009) suggests that the majority of excitatory inputs will be from nearby neurons. Under these conditions, evoked L5 qEPSCs showed no difference between control and trained animals (control 19.6 ± 0.4 pA; 24 hrs SAT 19.85 ± 0.5 pA, Figure S4A-D).

To test whether L5 to L2 qEPSCs were increased after 24 hrs SAT, we expressed ChR2 specifically in L5 neurons using the Etv1-Cre driver line for ChR2 expression. A comparison of optogenetically-evoked L5 qEPSC amplitudes in L2 Pyr neurons showed no difference between control and trained animals (control 20.1 ± 1.1 pA; 24 hrs SAT 19.6 ± 1.4 pA; Figure S4E-H). QEPSCs in L2 Pyr neurons evoked using an extracellular stimulating electrode in L2 also did not show any increase in mean amplitude after 24 hrs of training (Figure S4I-K). These results suggest that the training-induced increase in POm-initiated spiking activity in L2 Pyr cannot easily be attributed to synaptic strengthening of intralaminar L5-L5 or translaminar L5 to L2 excitatory inputs, and that this activity is driven by increased L5 Pyr firing associated with potentiation of POm to L5 excitatory inputs.

Sensory stimulation alone does not drive POm plasticity

To determine whether POm to L5 synaptic changes were linked to learning, or more generally to stimulus exposure during the training period, we created a pseudotraining paradigm with identical trial and stimulus structure but with altered reward contingency such that the whisker stimulus no longer predicted reward (Figure 7A). Similar to SAT, we observed a transient dip in anticipatory lick rates following stimulation presentation early in training that rapidly recovered, indicating that the animals perceived the stimulus and rapidly habituated to it.

After 24 hrs of pseudotraining, animals displayed no difference in anticipatory licking behavior between stimulus trials and non-stimulus trials, as both trial types had a 50% chance of water delivery (Figure 7B,C). Importantly, the number of airpuff-exposed trials for pseudotrained animals was greater than the mean trial number for SAT animals (Figure 7C),

likely because water was only provided on 50% of trials, versus 80% during SAT, requiring more trials to receive the same amount of water.

To determine if synaptic strengthening of POM inputs in L5 Pyr neurons was specific to sensory learning or could occur with passive sensory stimulation, POM qEPSC input strength was recorded in pseudotrained animals. After 24 hrs, mean POM synaptic strength onto L5 neurons was unchanged from control values and significantly smaller than POM qEPSCs in animals that had undergone SAT (control 15.8 ± 0.53 pA; pseudotrained 15.8 ± 0.59 pA; Figure 7E-G). Thus, sensory stimulation decoupled from reward is not sufficient to drive POM thalamocortical plasticity at L5 Pyr neurons.

To determine whether POM input plasticity was specifically related to the rewarded whisker-deflection stimulus or might reflect the activation of non-specific sensory cues related to training, we replaced the airpuff with a different sensory stimulus, a 500 ms-long light flash followed by a 500 ms delay to water delivery (Figure S5A). The light flash was delivered unilaterally from a triggered LED at the same location as the airpuff in other trials, and generated a transient suppression in licking frequency at the onset of training indicating animal detection. However, association of the light flash with the water reward proved more difficult to acquire, as animals did not display a behavioral change in anticipatory licking even after 48 hrs of light-flash association training (Figure S5B). POM to L5 Pyr qEPSC amplitudes did not change with light association training (Figure S5D,E). These data indicate that POM input plasticity in S1 occurs only when the stimulus is both whisker-dependent and directly coupled to the water reward, and that non-tactile arousal or attentional cues are unlikely to explain the pathway-specific changes observed.

Pathway-specific changes in L2 Pyr neurons after SAT

The absence of plasticity at POM inputs to L2 Pyr neurons after 24 hrs SAT might suggest that the conditions required for synaptic potentiation have not yet been met, or it could mean that L2 neurons do not possess the machinery for learning-dependent synaptic plasticity. To test whether longer periods of SAT might be sufficient to change POM input strength in L2 Pyr neurons, we examined ChR2-evoked POM-mediated qEPSC amplitudes at a later time point. After 48 hrs of SAT, task performance was further enhanced, driven primarily by an increase in stimulus-associated licking and not a depression of licking in blank trials (Figure 8B,C).

After 48 hrs SAT, qEPSC amplitude of POM to L2 Pyr neurons was significantly increased (control 17.8 ± 0.77 pA; 48 hrs SAT 22.2 ± 0.49 pA; Figure 8D-G). The increase in POM input to L2 Pyr was not matched by a further enhancement of POM input strength onto L5 Pyr (Figure 8H-K). Did this increase in POM response amplitude in L2 require 2 days of SAT, or might it be a time-dependent process initiated during the first 24 hours after training? To test this possibility, animals were trained for 24 hrs and then allowed to drink ad lib from the lickport without airpuff stimulation for an additional 24 hours. In this group, POM to L2 qEPSC amplitude was unchanged from control (control 17.8 ± 0.77 pA; 2 hrs SAT plus 24 hrs no stimulation 16.8 ± 0.43 pA, $n=10$ cells, $N=4$ animals).

Taken together, these data indicate that the absence of POM thalamocortical plasticity in L2 Pyr at 24 hrs SAT is not dependent on time since training initiation. Rather, we find that continuous training is important, and 48 hrs of sensory association is sufficient to increase POM input strength onto L2 Pyr neurons.

Synaptic plasticity between L2 Pyr neurons in barrel cortex has been well-documented, both in acute brain slices and after *in vivo* sensory experience (Albieri et al., 2015; Cheetham et al., 2008; Rodríguez-Moreno and Paulsen, 2008; Wen and Barth, 2011); however, rewiring of this local network has not been linked to sensory learning. To determine whether POM thalamocortical plasticity during SAT occurred concurrent with changes in the L2 excitatory network, we examined changes in qEPSC amplitudes after 48 hrs SAT measured from local afferent stimulation, using an extracellular electrode placed in L2. At this stage, qEPSC amplitudes were significantly increased in L2 Pyr neurons compared to control and 24 hr values (Figure S4I-L).

We also examined whether L5 to L2 or L5 to L5 qEPSC input strength might also increase after 48 hrs of SAT, but did not detect a change in either pathway (Figure S4A-H). Overall, these data show that SAT-initiated increases in L2 excitatory strength are delayed with respect to L5, and that L2 synaptic potentiation may be pathway-specific, detectable at thalamocortical but not within the aggregate excitatory input to L2 and L5a Pyr neurons after 48 hrs of SAT.

We also examined the relationship between mean qEPSC amplitude for a given animal and metrics for trial completion and task performance (anticipatory licking) during SAT. No statistically-significant, positive relationship between increased qEPSC amplitude and number of trials or animal performance was observed at either 24 or 48 hrs SAT, for L2 and L5 Pyr neurons (Figure S6). However, qEPSC values can differ widely across cells even within an animal, and in some cases we had only a single qEPSC measurement from a given subject. Interestingly, POM input strength at L2 synapses was negatively correlated with animal trial number at 48 hrs of SAT ($p=0.002$), suggesting a possible activity-dependent depotentiation (Clem et al., 2008).

Discussion

We aimed to develop a comprehensive account of how a learned sensory-association task alters synaptic function in neocortical circuits, with isolation of specific input pathways and targeted recordings from specific cell types across different layers of the cortex. High-throughput, home-cage sensory-association learning revealed that thalamocortical synapses are a site of early synaptic change in primary somatosensory cortex, with selectivity for POM but not VPM-related pathways. Synaptic potentiation at POM inputs onto L5 Pyr neurons was then followed by POM input potentiation to L2 Pyr neurons and within the L2 excitatory circuit over subsequent days of training. Importantly, changes were not observed with pseudo-conditioning, indicating that they were not driven by sensory stimulation alone. These data show that sensory association training drives sequential changes in excitatory synaptic strength in an input- and layer specific manner, and lay a foundation for understanding how learning alters the flow of information across the cortical column.

Thalamocortical plasticity during learning

Thalamocortical connections, particularly from VPM to L4, have been considered the major source of cortical input to somatosensory cortex, although there is an increasing awareness that POM inputs also provide significant drive (Audette et al., 2017; Gambino et al., 2014; Jouhanneau et al., 2014; Mease et al., 2016). Abundant experimental evidence indicates VPM inputs are resistant to experience-dependent alterations after the early postnatal period (Feldman and Brecht, 2005). However, prior studies have largely ignored the potential role of POM in neocortical response plasticity. We used pathway-specific activation of VPM and POM thalamic inputs and targeted recordings in the cortex as a screen for learning-related changes across the cortical column. VPM-evoked cortical firing was remarkably stable after early sensory association training in L4 and L5, as well as in the downstream target L2/3. In contrast, POM-evoked firing was dramatically increased. POM input plasticity may contribute to increased evoked firing in L5 Pyr neurons following sensory experience (Diamond et al., 1994; Jacob et al., 2012; Ward et al., 2012b).

What might explain the difference in plasticity between VPM and POM pathways? L4 neurons may be particularly resistant to post-critical period plasticity (Crair and Malenka, 1995; Fox, 1992), but we did not observe enhanced firing elsewhere in the VPM pathway, for Pyr neurons in L2/3 and L5. Although we cannot rule out target-specific changes in VPM input strength – for example, opposite changes in VPM drive to excitatory and inhibitory neurons that result in no net change in firing output – our assay clearly revealed an increase in response output in POM-recipient layers. Differences in plasticity induction could be attributed to the pattern or duration of sensory-evoked activity in VPM and POM during sensory stimulation (Sobolewski et al., 2015). Because POM is more strongly influenced by descending cortical drive than VPM, it is possible that recurrent corticothalamic circuitry may prime POM circuits for learning-dependent plasticity. Finally, our assay revealed differences between VPM and POM-evoked intracortical dynamics. Optogenetic activation of VPM inputs never evoked prolonged depolarization in any cortical layers, whereas POM activation frequently did. This sub-and suprathreshold activity may be permissive to plasticity induction that is specific to POM-recipient circuitry.

The capacity for learning-induced strengthening of thalamic inputs, while unexpected in the sensory cortex, has been previously described in the motor cortex (Biane et al., 2016). Rapid learning-related thalamic input plasticity may be an important feature of analogous higher-order sensory thalamic nuclei, such as the pulvinar (Arcaro et al., 2015; Purushothaman et al., 2012; Roth et al., 2016).

Sequence for cortical rewiring during sensory learning

Behavioral evidence for learning emerged early during SAT and performance increased with longer training periods, a slow trajectory of learning that enabled identification of progressive synaptic changes in the neocortex. Increased POM-evoked firing in both deep and superficial layers occurred at the same time as synaptic strengthening of POM inputs to L5 Pyr neurons, after only 24 hrs of training. The short latency of evoked spikes and the absence of enhanced excitability in L5 Pyr suggests synaptic strengthening at POM inputs

to L5 Pyr drove the increase in spiking. Although L2 Pyr neurons also showed an increase in POM-evoked firing after 24 hrs of SAT, synaptic changes at thalamic or intracortical inputs to L2 were absent and slice transection data indicates that this increased drive was indirect, arising from ascending input from infragranular layers. However, 48 hrs of SAT was sufficient to drive both POM to L2 Pyr synaptic strengthening as well as intralaminar plasticity in local L2 excitatory circuits.

Why was synaptic plasticity in L2 delayed relative to POM plasticity in L5? One possibility is that activity levels in superficial layers of the sensory cortex are too low initially to engage activity-dependent plasticity mechanisms. It is therefore notable that the increase in POM-evoked activity in L2 is evident prior to any observable change in synaptic strength in these neurons. Early synaptic strengthening in the more robustly active L5 could play a role in enhancing stimulus-evoked activity in L2 and drive POM input potentiation. Our results identify POM thalamic inputs to L5 as the cortical ‘first responder’ for training-evoked cortical plasticity. It will be of great interest to identify the dependent processes that underlie the sequential pattern of cortical changes revealed in this study.

Notably, we did not find evidence for synaptic potentiation at translaminar L5 to L2 synapses, nor within the L5 excitatory circuit, despite well-documented anatomical pathways and prior experimental evidence that these connections can be plastic under some circumstances (Sjöström and Häusser, 2006). Our assays may have been too coarse to detect subtle changes between specific subtypes of L5 Pyr neurons, or opposing changes within the same pathway. Learning-dependent changes in inhibitory synapses will be an important direction of future investigations.

Learning-related changes in neocortical circuits

POM-related synaptic changes, despite proceeding at the same timescale as behavioral learning, could have been generated by repeated sensory stimulation rather than learning. Although the airpuff stimulus is likely to be particularly salient and thus a good activator of POM circuits (Jouhanneau et al., 2014; Sosnik et al., 2001), it is notable that pseudoconditioning did not generate any change in POM input strength in L5 Pyr despite delivering the same or even a greater number of airpuff stimuli to animals, decoupled from a water reward. These findings indicate that synaptic plasticity in primary sensory cortex is strongly influenced by contingent reward, not just stimulus exposure.

Do cortical synaptic changes relate to sensory perception and task performance? POM input strength and task performance were not significantly correlated, possibly due to high variability in qEPSC measurements which were often averaged from a small number of cells per animal due to the difficulty of obtaining these data from a given animal. However, the weak relationship between qEPSC values and the number of training trials suggests a progressive link between stimulus-reward associations and the degree of synaptic strengthening at POM inputs.

Wide-ranging approaches suggest varied, and often contradictory, locations and mechanisms underlying perceptual and associative learning, but perceptual learning has been more

closely linked to changes in primary sensory cortex (Caras and Sanes, 2017; Makino et al., 2016; McGann, 2015). POM and analogous higher-order thalamic nuclei interface between primary sensory cortex, association cortex, motor cortex, and the striatum, making them well-positioned to integrate and transmit diverse information that may be important both for learning and initiation of cortical plasticity.

High-throughput, home-cage behavioral training

Analysis of learning-dependent reorganization of excitatory circuits across the cortical column with layer- and input-specific resolution was facilitated by a high-throughput home-cage training system, optimized for training large numbers of animals with minimal handling. Training occurred during the animal's normal active period and did not involve animal handling, a significant source of stress that may impair learning (Francis and Kanold, 2017). Sensory association training using a gentle airpuff stimulus drove progressive changes in behavior that occurred quickly enough to enable detailed electrophysiological investigation, but were slow enough to capture sequential changes in synaptic function across the cortical column (Poddar et al., 2013).

The training setup we developed was easily adapted to alter the contingency between water reward and conditioned stimulus for pseudotraining, and could be further modified to alter other task parameters such as reward valence, frequency, or sensory stimuli delivered. Home-cage training paradigms will be particularly useful for integrating cutting-edge recording, imaging, and stimulating technologies in freely-moving animals.

Conclusion

Our analysis of synaptic changes reveals the footprints of plasticity that are induced during an associative learning task that might be difficult to isolate during dynamic recording of neural activity. Importantly, our study did not address how SAT activates thalamic and neocortical neurons *in vivo*, nor how it alters thalamic response properties after training. Future experiments with fine-scale cell-type and temporal resolution will illuminate how activity in VPM, POM, and specific layers of the neocortex are engaged by and changed during learning.

The progressive emergence of POM- plasticity at infragranular synapses, followed by POM input potentiation at L2 Pyr neurons and an increase in intralaminar L2-L2 excitatory synaptic strength suggests that supragranular layers may have a higher threshold but a large capacity for experience-dependent plasticity. These findings will be essential to develop and test data-constrained models of synaptic change and neural spiking.

STAR Methods

Contact for Reagent and Resource Sharing

Further information and requests for resources and reagents should be directed to and will be fulfilled by the Lead Contact, Alison L. Barth (albarth@andrew.cmu.edu).

Experimental Model and Subject Details

Animals—All experimental procedures were conducted in accordance with the NIH guidelines and were approved by the Institutional Animal Care and Use Committee at Carnegie Mellon University.

Experiments targeting excitatory neurons were performed on C57Bl6 mice (Harlan). In a small subset of experiments, ChR2 expression was driven transgenically by crossing Nelf1Cre (Gong et al., 2007)(MMRC Stock No: 037424-UCD) animals or ETV1creER (Gong et al., 2007; Taniguchi et al., 2011) (Jackson Laboratory Stock No: 013048) animals with Ai32 (Jackson Laboratory Stock No. 024109, ChR2(H134R)EYFP) animals to generate offspring that express ChR2 specifically in VPM and L5Pyr neurons respectively. ETV1-Cre expression was initiated by injection of 2mg tamoxifen (100uL of 20mg/ml, Tocris Cat No 6342, <https://www.jax.org/research-and-faculty/tools/cre-repository/tamoxifen>) 8-12 days before behavioral training. We observed broad expression of ChR2 across the entire extent of L5 in these animals. Experiments were performed on animals of both sexes. Animals were stereotaxically injected between postnatal day 12-18 (P12-18), began training at P19-28, and were sacrificed for recording at P20-P30.

Method Details

Viral Injections—ChR2 tagged with m-cherry or YFP (300-500 nl; AAV1.CAG.hChR2(H134R)-mCherry.WPRE.SV40, Catalog No. 100054-AAV1, Addgene, Cambridge, MA; AAV2-hSyn-hChR2(H134R)-EYFP, Deisseroth Lab, UNC Vector Core, Chapel Hill, NC) was stereotaxically injected into the VPM or POM thalamic nucleus following a small craniotomy (VPM: bregma -1.3, lateral 1.8, depth 3.4, POM: bregma -1.7, lateral 1.00, depth 3.25 mm) of isoflurane-anaesthetized mice using a Hamilton syringe (Hamilton; Reno, NV), Stoelting infusion pump (Stoelting; Wood Dale, IL, Model #53210), and custom injection cannulas (Plastics One; Phoenix, AZ). Mice were treated once with ketoprofen after injection (5 mg/kg, Sigma-Aldrich; St. Louis, MO) and additional doses were administered as necessary. Mice recovered in their home cage for 7-13 days prior to sensory association training (SAT).

Automated home-cage sensory association training—Animals were singly housed in a 7x12 cm standard mouse cage outfitted with a custom-designed chamber with an infrared beam-break in front of a recessed lickport with a capacitor to detect individual lick events. Animals were maintained on a 12 hour light-dark schedule, with lights on at 7 am. The lickport was the sole source of water in the cage, and animals were not otherwise water restricted. Food was provided ad libitum. Animals were typically introduced to the training cage at noon and allowed one day to acclimate to the cage. They readily learned to drink at the lickport without intervention or shaping, where ~1-3 mls of water were dispensed each day. Water was provided on 80% of the beambreak-initiated trials, without any predictive cue on the acclimation day. At noon on the second day, a small nozzle for air delivery (inner diameter 1/16 in) was inserted into the ceiling of the chamber ~ 4 cm above the average location of the right vibrissa during drinking. Mouse position for the airpuff was not stereotyped, and the number and amplitude of whisker movements evoked were not monitored.

We elected to use a gentle airpuff as the stimulus in our sensory association task for several reasons. First, airpuff stimuli can target multiple whiskers without whisker contact, well-suited for automated home-cage-training. Second, animals can be directly introduced to the training cage without whisker trimming or whisker prostheses that can be difficult to maintain over long training periods. Third, because multiple whiskers can be stimulated in a single trial, the cortical region for analysis encompasses a wide area of S1, facilitating fine-scale analysis in acute brain slices (in comparison to single-whisker stimulation paradigms).

For all trials, including during acclimation, IR beam break triggered a variable delay (200-800ms) before trial initiation, after which the nozzle delivered a short (500 ms) pulse of compressed air at 4-6 psi (measured by a gas regulator). Water was delivered 500 ms after the airpuff offset (1s after trial start), and approximately 50 μ l of water was dispensed for each trial. Airpuffs and water were delivered as described for 80% of the beambreak-initiated trials (a random number between 0 and 100 was generated and if it was less than 80, water was delivered). The remaining 20% of trials had no airpuff and no water delivery but otherwise had identical trial structure and incidental auditory cues, including variable pre-trial delay. After trial initiation, a new trial could not be triggered until 1s after water delivery, and additional IR beam breaks during the trial were ignored. In a subset of experiments, mice received an identical training paradigm but using a visible light-flash as the conditioned stimulus. The light flash was broad spectrum and directed downwards into the drinking area from above on the right side of the drinking chamber. In an additional subset of experiments, mice received a pseudo-training paradigm which was identical to the previously described trial structure except that water was delivered on 50% of trials randomly determined irrespective of stimulus delivery. All animals performed either 25 or 150 trials, so a small minority of animals that failed to perform 25 trials was excluded from analysis.

Data was analyzed in Matlab and excel using custom scripts that align measured licks to individual trials and measure the delay from trial start for each lick. The presence of a lick was determined by a change in capacitance at the lickport, surveyed in 100 ms time bins surrounding water delivery. PSTHs of lick behavior were generated relative to trial start (following the initial delay) so that changes in licking behavior could be aligned to CS and US delivery. To quantitate learning-related behavioral changes, lick rates were compared between water or stimulus trials to lick rates for no-water “blank” trials on Day 0 and in the last 8 hrs of training day 1 or 2. We differentiated between consummatory licking (required for water consumption) and anticipatory licking prior to water delivery (evidence that an association between the sensory stimulus and the prediction of a future water “reward”) (Cohen et al., 2012). Anticipatory lick events (occurring 300 ms preceding water delivery, 700-1000 ms after $t=0$) were measured throughout training in 4 hour bins for water-delivery trials and for blank trials. Lick frequency calculated over 100 ms time bins within this window were then converted into Hz.

To quantitate learning-related behavioral changes, lick rates were compared between water or stimulus trials to lick rates for no-water “blank” trials (100ms bins) on Day 0 and in the last 8 hrs of training day 1 or 2. We differentiated between consummatory licking (required for water consumption) and anticipatory licking prior to water delivery (evidence that an

association between the sensory stimulus and the prediction of a future water “reward”) (Cohen et al., 2012). Anticipatory lick events (3, 100 ms time bins sampled for 300 ms preceding water delivery, 700-1000 ms after $t=0$) were measured throughout training in 4 hour bins for water-delivery trials and for blank trials. Lick frequency calculated over 100 ms time bins within this window were then converted into Hz. Performance was defined as the difference between lick rate for stimulus and blank trials, which was measured and plotted in 4 hour time bins. Regression of electrophysiology and behavior utilized each animal’s performance quantified for the last 20% of trials performed. All measurements of behavior were calculated for individual animals and then combined to generate aggregate values.

Slice Preparation and Injection Site Confirmation—Injected mice were sacrificed by brief isoflurane anesthesia and decapitation between 11am and 3pm. 350 μ m thick off-coronal slices (One cut, 45° rostral-lateral and 25° rostral-dorsal) designed to preserve columnar connections in the somatosensory cortex were prepared in ice-cold artificial cerebrospinal fluid (ACSF) composed of (in mM): 119 NaCl, 3.5 KCl, 1 NaH₂PO₄, 26.2 NaHCO₃, 11 glucose, 1.3 MgSO₄, and 2.5 CaCl₂ equilibrated with 95%/5% O₂/CO₂. Slices were allowed to recover at room temperature for 45 minutes in the dark before recording. The injection site was confirmed anatomically using the mCherry-tagged ChR2 fluorescence in cell bodies at the injection site and the characteristic pattern of fluorescent axonal labeling in the barrel cortex, concentrated in L4 and L6 for VPM and L1 and L5a for POM (Meyer et al., 2010). Slices that had fluorescently labeled axons outside of the target layers were discarded. Retrogradely-labeled, ChR2⁺ neurons were not observed in the somatosensory cortex.

Although ChR2 expression levels could differ between animals, experiments were repeated across many animals, mice were assigned to experimental groups without expression information, and all controllable experimental variables were kept consistent. Additionally, fluorescent ChR2 labeling in the cortex was monitored. A consistent minimum expression threshold for inclusion was applied, and no difference was observed in the mean or range of fluorescent intensity between control and trained animals.

General Electrophysiology—Cortical excitatory neurons were targeted for whole-cell recording in the posteromedial barrel subfield using an Olympus light microscope (BX51WI) using borosilicate glass electrodes resistance 4-8 M Ω . Electrode internal solution for evoked activity experiments, was composed of (in mM): 125 potassium gluconate, 10 HEPES, 2 KCl, 0.5 EGTA, 4 Mg-ATP, and 0.3 Na-GTP, pH 7.25-7.30, 280 mOsm. Internal solution for quantal EPSC experiments was composed of (in mM) 130 cesium gluconate, 10 HEPES, 0.5 EGTA, 8 NaCl, 10 Tetraethylammonium chloride (TEA-Cl), 4 Mg-ATP and 0.4 Na-GTP, pH 7.25-7.30, 280-290 mOsm and typically contained QX-314 (5mM, lidocaine N-ethyl bromide, Tocris). For some cells trace amounts of AlexaFluor 594 were added to the internal solution to confirm cell targeting.

Electrophysiological data were acquired using a Multiclamp 700A amplifier (Axon Instruments, Foster City, CA) and a National Instruments acquisition interface (National Instruments; Austin, TX). Data were filtered at 3 kHz, digitized at 10 kHz and collected

by Igor Pro 6.0 (Wavemetrics, Lake Oswego, Oregon). Cells were allowed to recover from break-in for 5 minutes before data collection. Presumptive excitatory neurons were targeted for whole-cell or juxtacellular recording based on Pyr soma morphology (or stellate nature morphology in L4), intermediate Ri, ($354 \pm 23 \text{ M}\Omega$), and regular-spiking phenotypes in response to current injections. Input-output firing curves were generated from neurons recorded in a potassium-gluconate based internal solution by injecting increasing amplitudes of a square pulse of current to elicit spikes. To ensure that potential changes in spontaneous synaptic currents did not influence measured intrinsic property values, we also recorded resting membrane potential and input-output curves in the presence of synaptic blockers for a subset of neurons control and SAT24 animals. We observed no difference across recording condition and data was pooled for further analysis. Rs and Ri were monitored for the duration of experiments and cells with Ri below $100 \text{ M}\Omega$, Rs greater than $40 \text{ M}\Omega$, or where Rs changed by more than 30% over the course of data collection were excluded from further analysis.

Following recording, cells were imaged to determine their laminar location based on depth from pial surface and relevant cytoarchitectural features. L2 neurons were defined as neurons up to $100 \text{ }\mu\text{m}$ below the cell-sparse area of L1, typically $50\text{-}150 \text{ }\mu\text{m}$ below the pial surface. L4 neurons are defined as inside the upper and lower limit of the L4 barrel, but were selected from both “barrel” and “septal” regions, since segregated barrel and septal circuits in mouse L4 are unclear (Feldmeyer et al., 2013). L5 neurons were recorded from the area up to $150\text{ }\mu\text{m}$ below L4 barrels, an area corresponding to L5a.

Evoked cortical activity—ChR2-expressing thalamic axons were stimulated by delivering trains of light pulses (5 pulses, 80ms ISI, 0.05Hz inter-trial interval) through a $40\times$ water-immersion objective (Olympus) at the recording site using a white LED (Prizmatix, Israel) in combination with an excitation filter (40nm bandwidth centered at 480nm ; Chroma; Bellows Falls, VT). Max light intensity at 470 nm was measured at 2.13 mW distributed over a beam area $\sim 1 \text{ mm}$ diameter, and the timing of optogenetic stimulation was controlled by a Master-8 (A.M.P.I; Jerusalem, Israel). Responses in excitatory cortical neurons were measured in either the whole cell or juxtacellular configuration in a modified ACSF solution identical to cutting solution but with (in Mm) 2.5cvKCl , 0.5 MgSO_4 , and 1 CaCl_2 (Audette et al., 2017).

Spike data from at least 10 consecutive trials for each cell was binned at 10ms intervals and averaged across all cells of a given population to generate an average PSTH. The average firing rate was calculated for 500ms pre-stim, during stim, and post-stim. A cell was included in the fraction of spiking cells if any action potential(s) was observed in the stimulus or post-stimulus window. Evoked activity experiments were performed for control animals, which had undergone at least one day of cage acclimation but received no sensory stimuli, and for animals that had undergone 24 hrs of sensory association training.

In a subset of experiments, POM- evoked activity in L2 pyramidal neurons was recorded from 24 hrs SAT animals before and after making an incision through L4. Incisions of $1\text{-}2\text{mm}$ were manually performed with a custom knife. For each post-incision L2 cell to be included in analysis, an adjacent pre-cut cell was recorded to insure that the slice

had sufficient ChR2 expression to drive cortical activity. Evoked activity was measured as previously describe. To insure that our incision did not fundamentally alter the direct POM input onto L2 Pyr neurons, the onset latency and slope of the earliest identifiable POM-evoked EPSP were measured. The slope of the initial rise was defined as the maximum slope before a second inflection point.

Synaptic analysis—Subthreshold excitatory post-synaptic potentials were calculated for Pom- and VPM-evoked current clamp recordings made from control and SAT24 animals. For each cell, trials that did not contain an action potential in response to the first light pulse were averaged together to create an average of sub-threshold responses. Peak EPSP amplitude within 20 ms of the first light stimulus was then measured for each cell average trace. In many cells, especially after training, optogenetic stimulation of POM inputs drove action potentials on every trial, so PSPs could not be isolated, particularly for cells that had the largest PSPs. Additionally, measured subthreshold EPSPs likely represent a composite of thalamic and local inputs since optical activation of thalamic inputs can drive rapid action potential generation in some cortical populations that feedback upon the recorded neuron. Peak subthreshold amplitudes of cell average responses in the one second following stimulus train offset (500-1500ms after stimulus onset) were also measured to assess prolonged depolarization.

In a subset of experiments, thalamically evoked cortical responses were recorded in voltage clamp to assess paired pulse ratio and AMPA:NMDA ratio. For paired pulse experiments, neural responses to trains of light pulses (5 pulses, 80ms ISI, 0.05Hz inter-trial interval) were recorded at -70mV (E_{Cl^-}). Paired pulse ratio was measured as the peak amplitude of the cell average response within 20ms of the second light pulse divided by the peak amplitude of the cell average response within 20ms of the first light pulse. For AMPAR:NMDAR current ratio experiments, stimulus intensity was reduced to avoid polysynaptic activity that would contaminate accurate measurements of the direct POM response. Because this measurement is a ratio, it is independent of stimulus intensity and could thus be used across different slice preparations. EPSCs to a single light pulse were recorded at -70mV (AMPA) and $+40\text{mV}$ (NMDA) in the presence of picrotoxin to block disynaptic thalamically-evoked inhibition. Light pulse duration and intensity were titrated for each cell to produce a response with minimal polysynaptic activity. The amplitude of the AMPA component was measured as the peak amplitude of the cell average response within 20ms of the light pulse. The NMDA response was measured as the amplitude of the cell average response 50ms after the light pulse to ensure that the AMPA component of the response had returned to baseline.

Input-specific quantal EPSC measurements—Quantal amplitude measurements were performed in the standard ACSF solution used during cutting but containing SrCl_2 instead of CaCl_2 and in the presence of the NMDA receptor antagonist AP5 (50 μM , Tocris Catalog No. 0106, Minneapolis, MN). Well-isolated individual quantal EPSCs were recorded at -70mV following input-specific optical stimulation (1 pulse, 5ms, variable intensity) of ChR2-expressing axons (Biane et al., 2016; Wen and Barth, 2011). Quantal events were manually selected but blind to cell identity based on their short rise time,

isolated baselines, and absence of multiple inflection points indicative of a compound event. Events occurring between 50 and 500ms following stimulation (minimum of 25 per cell) were analyzed using MiniAnalysis software (Synaptosoft, Decatur, GA; Detection parameters: Threshold 9pA; local maximum period 3.5ms; baseline period 6ms; decay time period 10ms; decay time fraction 0.333; baseline average period 4ms; area threshold 10 pA; peak average points 3) aligned to rise, and averaged to generate an average qEPSC trace for each cell. The average qEPSC trace for each cell in an experimental group was then aligned to rise to generate a global qEPSC amplitude. The amplitude of each event was averaged to determine a cell's average qEPSC amplitude and cumulative distribution histograms were generated from a pool of qEPSCs containing 25 randomly selected events from each cell in an experimental group. Since the amplitude of quantal events can be influenced by Rs, only cells below 25 MΩ were included. Experiments in ETV1Cre mice were performed in the presence of the GABA_A receptor antagonist Picrotoxon (50uM, Tocris, Cat. No. 1128) due to a small number of inhibitory neurons in the ETV1-Cre expressing population (Lu et al., 2017). L2-L2 and L5-L5 connections were stimulated using a concentric bipolar stimulating electrode (FHC Catalog No. CBCRC75, Bowdoin, ME) placed in L2 or L5 100-400 uM away from the recorded neuron. For qEPSC experiments, light or electrical stimulus intensity was low and calibrated individually for each cell to evoke an initial multiquantal EPSC between 50 and 150pA.

Quantification and Statistical Analysis

Unless specifically noted in figure legend, calculations and statistics were performed on cells and all statistical tests are non-parametric Mann-Whitney (unpaired) or Wilcoxon (paired) rank sum tests, and significance values are reported in figure or when references in results. All average values are mean ± SEM unless indicated. Cell (n) and animal values (N) are reported in each figure. Animals were randomly assigned to experimental group, and quantal amplitude experiments were analyzed blind to cell identity. Potential relationships between trial number, performance (L_w-L_b), and qEPSC amplitude were plotted and evaluated using a Spearman rank-order correlation test. Analysis of qEPSC amplitude versus performance included some animals that did not show an increase in L_w-L_b; thus, the regression analysis included performance values that were <0. Because we did not have lick frequency data for a subset of animals that went through SAT, the number of points differs for the regression of qEPSC amplitude and trial number versus qEPSC value and performance.

Supplementary Material

Refer to Web version on PubMed Central for supplementary material.

Acknowledgements

Special thanks to Joanne Steinmiller for expert animal care, Rogan Grant, Zhuopin Sun, Alex Hsu and Megumi Matsushita for technical assistance, and members of the Barth Lab for helpful comments. Special thanks also to Joanna Urban-Ciecko for essential contributions to the revised manuscript. This work was supported by the Carnegie Mellon University Hillman Presidential Fellowship (N.J.A.), the IISC-CMU BrainHub postdoctoral fellowship (A.R) and NIH R01NS088958. (to A.L.B.).

References

- Albieri G, Barnes SJ, De Celis Alonso B, Cheetham CEJ, Edwards CE, Lowe AS, Karunaratne H, Dear JP, Lee KC, and Finnerty GT (2015). Rapid bidirectional reorganization of cortical microcircuits. *Cereb. Cortex* 25, 3025–3035. [PubMed: 24836895]
- Alloway KD, Hoffer ZS, and Hoover JE (2003). Quantitative comparisons of corticothalamic topography within the ventrobasal complex and the posterior nucleus of the rodent thalamus. *Brain Res* 968, 54–68. [PubMed: 12644264]
- Arcaro MJ, Pinsk MA, and Kastner S (2015). The Anatomical and Functional Organization of the Human Visual Pulvinar. *J. Neurosci* 35, 9848–9871. [PubMed: 26156987]
- Audette NJ, Urban-Ciecko J, Matsushita M, and Barth AL (2017). P_{OM} Thalamocortical Input Drives Layer-Specific Microcircuits in Somatosensory Cortex. *Cereb. Cortex* 1–17. [PubMed: 28365777]
- Banerjee A, Meredith RM, Rodríguez-Moreno A, Mierau SB, Auberson YP, and Paulsen O (2009). Double dissociation of spike timing-dependent potentiation and depression by subunit-preferring NMDA receptor antagonists in mouse barrel cortex. *Cereb. Cortex* 19, 2959–2969. [PubMed: 19363149]
- Biane JS, Takashima Y, Scanziani M, Conner JM, and Tuszyński MH (2016). Thalamocortical Projections onto Behaviorally Relevant Neurons Exhibit Plasticity during Adult Motor Learning. *Neuron* 89, 1173–1179. [PubMed: 26948893]
- Bureau I, Von Paul F Saint, and Svoboda K (2006). Interdigitated paralemniscal and lemniscal pathways in the mouse barrel cortex. *PLoS Biol* 4, 2361–2371.
- Caras ML, and Sanes DH (2017). Top-down modulation of sensory cortex gates perceptual learning. *Proc. Natl. Acad. Sci* 114, 201712305.
- Chandrasekaran S, Navlakha S, Audette NJ, McCreary DD, Suhan J, Bar-Joseph Z, and Barth AL (2015). Unbiased, High-Throughput Electron Microscopy Analysis of Experience-Dependent Synaptic Changes in the Neocortex. *J. Neurosci* 35, 16450–16462. [PubMed: 26674870]
- Cheetham CEJ, Hammond MSL, McFarlane R, and Finnerty GT (2008). Altered Sensory Experience Induces Targeted Rewiring of Local Excitatory Connections in Mature Neocortex. *J. Neurosci* 28, 9249–9260. [PubMed: 18784305]
- Clem RL (2010). Ongoing in Vivo Experience in the Neocortex. *Science* (80-.). 101, 101–105.
- Clem RL, and Barth A (2006). Pathway-specific trafficking of native AMPARs by in vivo experience. *Neuron* 49, 663–670. [PubMed: 16504942]
- Cohen JY, Haesler S, Vong L, Lowell BB, and Uchida N (2012). Neuron-type-specific signals for reward and punishment in the ventral tegmental area. *Nature* 482, 85–88. [PubMed: 22258508]
- Crair MC, and Malenka RC (1995). A critical period for long-term potentiation at thalamocortical synapses. *Nature* 375, 325–328. [PubMed: 7753197]
- Cruikshank SJ, Urabe H, Nurmikko AV, and Connors BW (2010). Pathway-Specific Feedforward Circuits between Thalamus and Neocortex Revealed by Selective Optical Stimulation of Axons. *Neuron* 65, 230–245. [PubMed: 20152129]
- Diamond ME, Huang W, and Ebner FF (1994). Laminar Comparison of Somatosensory Cortical Plasticity Author (s): Diamond Mathew E., Huang Wei and Ebner Ford F. Published by : American Association for the Advancement of Science Stable URL : <http://www.jstor.org/stable/2884667> JSTOR is a not-for-. *Science* (80-.). 265, 1885–1888.
- Feldman DE, and Brecht M (2005). Map plasticity in somatosensory cortex. *Science* (80-.). 310, 810–815.
- Feldmeyer D, Brecht M, Helmchen F, Petersen CCH, Poulet JFA, Staiger JF, Luhmann HJ, and Schwarz C (2013). Barrel cortex function. *Prog. Neurobiol* 103, 3–27. [PubMed: 23195880]
- Fox K (1992). A critical period for experience-dependent synaptic plasticity in rat barrel cortex. *J. Neurosci* 12, 1826–1838. [PubMed: 1578273]
- Francis NA, and Kanold PO (2017). Automated Operant Conditioning in the Mouse Home Cage. *Front. Neural Circuits* 11, 1–6. [PubMed: 28174523]
- Galvez R (2006). Vibrissa-Signaled Eyeblink Conditioning Induces Somatosensory Cortical Plasticity. *J. Neurosci* 26, 6062–6068. [PubMed: 16738249]

- Gambino F, Pagès S, Kehayas V, Baptista D, Tatti R, Carleton A, and Holtmaat A (2014). Sensory-evoked LTP driven by dendritic plateau potentials in vivo. *Nature* 515, 116–119. [PubMed: 25174710]
- Glazewski S, and Barth AL (2015). Stimulus intensity determines experience-dependent modifications in neocortical neuron firing rates. *Eur. J. Neurosci* 41, 410–419. [PubMed: 25546174]
- Glazewski S, and Fox K (1996). Time course of experience-dependent synaptic potentiation and depression in barrel cortex of adolescent rats. *J. Neurophysiol* 75, 1714–1729. [PubMed: 8727408]
- Gong S, Doughty M, Harbaugh CR, Cummins A, Hatten ME, Heintz N, and Gerfen CR (2007). Targeting Cre recombinase to specific neuron populations with bacterial artificial chromosome constructs. *J. Neurosci* 27, 9817–9823. [PubMed: 17855595]
- Groh A, Bokor H, Mease RA, Plattner VM, Hangya B, Stroh A, Deschenes M, and Acsády L (2014). Convergence of cortical and sensory driver inputs on single thalamocortical cells. *Cereb. Cortex* 24, 3167–3179. [PubMed: 23825316]
- Harris J. a, Harris IM, and Diamond ME (2001). The topography of tactile working memory. *J. Neurosci* 21, 8262–8269. [PubMed: 11588197]
- Jacob V, Petreanu L, Wright N, Svoboda K, and Fox K (2012). Regular Spiking and Intrinsic Bursting Pyramidal Cells Show Orthogonal Forms of Experience-Dependent Plasticity in Layer V of Barrel Cortex. *Neuron* 73, 391–404. [PubMed: 22284191]
- Jouhanneau JS, Ferrarese L, Estebanez L, Audette NJ, Brecht M, Barth AL, and Poulet JFA (2014). Cortical fos GFP expression reveals broad receptive field excitatory neurons targeted by pom. *Neuron* 84, 1065–1078. [PubMed: 25453844]
- Karni A, and Sagi D (1991). Where practice makes perfect in texture discrimination: evidence for primary visual cortex plasticity. *Proc. Natl. Acad. Sci. U. S. A* 88, 4966–4970. [PubMed: 2052578]
- Kilgard MP (1998). Cortical Map Reorganization Enabled by Nucleus Basalis Activity. *Science* (80-.). 279, 1714–1718.
- Lambo ME, and Turrigiano GG (2013). Synaptic and Intrinsic Homeostatic Mechanisms Cooperate to Increase L2/3 Pyramidal Neuron Excitability during a Late Phase of Critical Period Plasticity. *J. Neurosci* 33, 8810–8819. [PubMed: 23678123]
- Lefort S, Tomm C, Floyd Sarria JC, and Petersen CCH (2009). The Excitatory Neuronal Network of the C2 Barrel Column in Mouse Primary Somatosensory Cortex. *Neuron* 61, 301–316. [PubMed: 19186171]
- Lu J, Tucciarone J, Padilla-Coreano N, He M, Gordon JA, and Josh Huang Z (2017). Selective inhibitory control of pyramidal neuron ensembles and cortical subnetworks by chandelier cells. *Nat. Neurosci* 20, 1377–1383. [PubMed: 28825718]
- Makino H, Hwang EJ, Hedrick NG, and Komiyama T (2016). Circuit Mechanisms of Sensorimotor Learning. *Neuron* 92, 705–721. [PubMed: 27883902]
- Masri R, Trageser JC, Bezdudnaya T, Li Y, Keller A, Trageser JC, Bezdudnaya T, and Li Y (2006). Cholinergic Regulation of the Posterior Medial Thalamic Nucleus. 2265–2273.
- McGann JP (2015). Associative learning and sensory neuroplasticity : how does it happen and what is it good for ? 567–576.
- Mease RA, Metz M, and Groh A (2016). Cortical Sensory Responses Are Enhanced by the Higher-Order Thalamus. *Cell Rep* 14, 208–215. [PubMed: 26748702]
- Meyer HS, Wimmer VC, Hemberger M, Bruno RM, De Kock CPJ, Frick A, Sakmann B, and Helmstaedter M (2010). Cell type-specific thalamic innervation in a column of rat vibrissal cortex. *Cereb. Cortex* 20, 2287–2303. [PubMed: 20534783]
- Mrsic-Flogel TD, Hofer SB, Ohki K, Reid RC, Bonhoeffer T, and Hübener M (2007). Homeostatic Regulation of Eye-Specific Responses in Visual Cortex during Ocular Dominance Plasticity. *Neuron* 54, 961–972. [PubMed: 17582335]
- Oberlaender M, Ramirez A, and Bruno RM (2012). Sensory Experience Restructures Thalamocortical Axons during Adulthood. *Neuron* 74, 648–655. [PubMed: 22632723]
- Petreanu L, Mao T, Sternson SM, and Svoboda K (2009). The subcellular organization of neocortical excitatory connections. *Nature* 457, 1142–1145. [PubMed: 19151697]
- Poddar R, Kawai R, and Ölveczky BP (2013). A fully automated high-throughput training system for rodents. *PLoS One* 8, 1–10.

- Porter JT, Johnson CK, and Agmon a (2001). Diverse types of interneurons generate thalamus-evoked feedforward inhibition in the mouse barrel cortex. *J. Neurosci* 21, 2699–2710. [PubMed: 11306623]
- Purushothaman G, Marion R, Li K, and Casagrande V. a (2012). Gating and control of primary visual cortex by pulvinar. *Nat. Neurosci* 15, 905–912. [PubMed: 22561455]
- Rioult-Pedotti MS, Friedman D, and Donoghue JP (2000). Learning-induced LTP in neocortex. *Science* (80-.). 290, 533–536.
- Rodríguez-Moreno A, and Paulsen O (2008). Spike timing-dependent long-term depression requires presynaptic NMDA receptors. *Nat. Neurosci* 11, 744–745. [PubMed: 18516036]
- Roth MM, Dahmen JC, Muir DR, Imhof F, Martini FJ, and Hofer SB (2016). Thalamic nuclei convey diverse contextual information to layer 1 of visual cortex. *Nat. Neurosci* 19, 299–307. [PubMed: 26691828]
- Schwartz S, Maquet P, and Frith C (2002). Neural correlates of perceptual learning : A functional MRI study of visual texture discrimination. 100, 1–6.
- Shibata K, Sasaki Y, Kawato M, and Watanabe T (2016). Neuroimaging evidence for 2 types of plasticity in association with visual perceptual learning. *Cereb. Cortex* 26, 3681–3689. [PubMed: 27298301]
- Sjöström PJ, and Häusser M (2006). A Cooperative Switch Determines the Sign of Synaptic Plasticity in Distal Dendrites of Neocortical Pyramidal Neurons. *Neuron* 51, 227–238. [PubMed: 16846857]
- Sobolewski A, Kublik E, Swiejkowski DA, Kami ski J, and Wróbel A (2015). Alertness opens the effective flow of sensory information through rat thalamic posterior nucleus. *Eur. J. Neurosci* 41, 1321–1331. [PubMed: 25912157]
- Sosnik R, Haidarliu S, and Ahissar E (2001). Temporal frequency of whisker movement. I. Representations in brain stem and thalamus. *J. Neurophysiol* 86, 339–353. [PubMed: 11431515]
- Summerfield C, Greene M, Wager T, Egner T, Hirsch J, and Mangels J (2006). Neocortical connectivity during episodic memory formation. *PLoS Biol* 4, 855–864.
- Taniguchi H, He M, Wu P, Kim S, Paik R, Sugino K, Kvitsani D, Fu Y, Lu J, Lin Y, et al. (2011). A Resource of Cre Driver Lines for Genetic Targeting of GABAergic Neurons in Cerebral Cortex. *Neuron* 71, 995–1013. [PubMed: 21943598]
- Urbain N, and Deschenes M (2007). A New Thalamic Pathway of Vibrissal Information Modulated by the Motor Cortex. *J. Neurosci* 27, 12407–12412. [PubMed: 17989305]
- Urban-Ciecko J, Fanselow EE, and Barth AL (2015). Neocortical somatostatin neurons reversibly silence excitatory transmission via GABA_B receptors. *Curr. Biol* 25, 722–731. [PubMed: 25728691]
- Viaene AN, Petrof I, and Sherman SM (2011). Properties of the thalamic projection from the posterior medial nucleus to primary and secondary somatosensory cortices in the mouse. *Proc. Natl. Acad. Sci* 108, 18156–18161. [PubMed: 22025694]
- Ward RL, Flores LC, and Disterhoft JF (2012a). Infragranular barrel cortex activity is enhanced with learning. *J. Neurophysiol* 108, 1278–1287. [PubMed: 22696544]
- Ward RL, Flores LC, and Disterhoft JF (2012b). Infragranular barrel cortex activity is enhanced with learning. *J. Neurophysiol* 108, 1278–1287. [PubMed: 22696544]
- Wen JA, and Barth AL (2011). Input-Specific Critical Periods for Experience-Dependent Plasticity in Layer 2/3 Pyramidal Neurons. *J. Neurosci* 31, 4456–4465. [PubMed: 21430146]
- Williams LE, and Holtmaat A (2019). Higher-Order Thalamocortical Inputs Gate Synaptic Article Higher-Order Thalamocortical Inputs Gate Synaptic Long-Term Potentiation via Disinhibition. *Neuron* 101, 91–102.e4. [PubMed: 30472077]

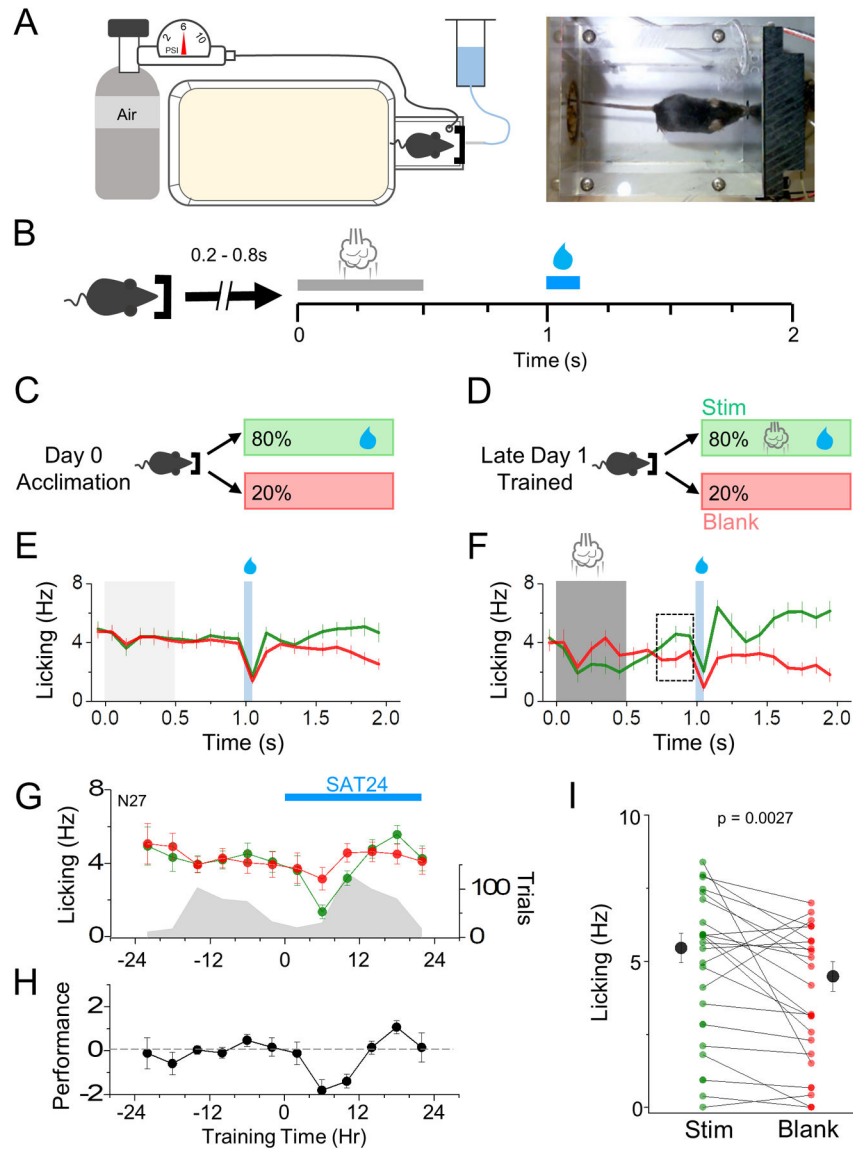


Figure 1. Automated home-cage training enables rapid acquisition of multi-whisker sensory association.

(A) Schematic of home-cage sensory association training cage (left) and image of mouse initiating a training trial (right). (B) Sensory association training paradigm. Upon IR beam-break measured nose poke, a random delay (200-800ms) occurs prior to trial initiation. Air puff delivery period (CS, 500ms duration, 4-6 PSI) occurs at $t=0$ following random delay with water delivery (US, 75ms, ~50 μ L) occurring at $t=1$ s, leaving a 500ms delay in between the CS and US. A new trial could not be initiated until $t=2$ s. (C,D) Identical trial structure during acclimation and SAT, with 80% of initiated trials providing water and air puff (no air puff during acclimation), and 20% of trials delivering neither air puff or water. (E,F) Average global lick rates (10ms bins) of mice during training trials on either acclimation day (E) or the last eight hrs (Hr 16-24) of training day 1 (F). Grey and white shading represent stimulus and water delivery, black box shows 300ms anticipatory lick window. $N=11$ animals for (E), (F). (G) Time course of anticipatory lick rates (left axis, 300ms prior

to water delivery, 4 hr bins) throughout training for blank (red) and stim/water trials (green) averaged across all animals. Trial initiation counts (right axis) are shown in grey for the same time bins. (H) Performance defined as the difference in anticipatory lick rates between stim/water trials and blank trials during learning. (I) Individual animal paired comparisons (Wilcoxin Rank Sum Test) of lick rate for stim/water trials and blank trials on the last 20% of trials on day 1. Averages represented as mean \pm SEM.

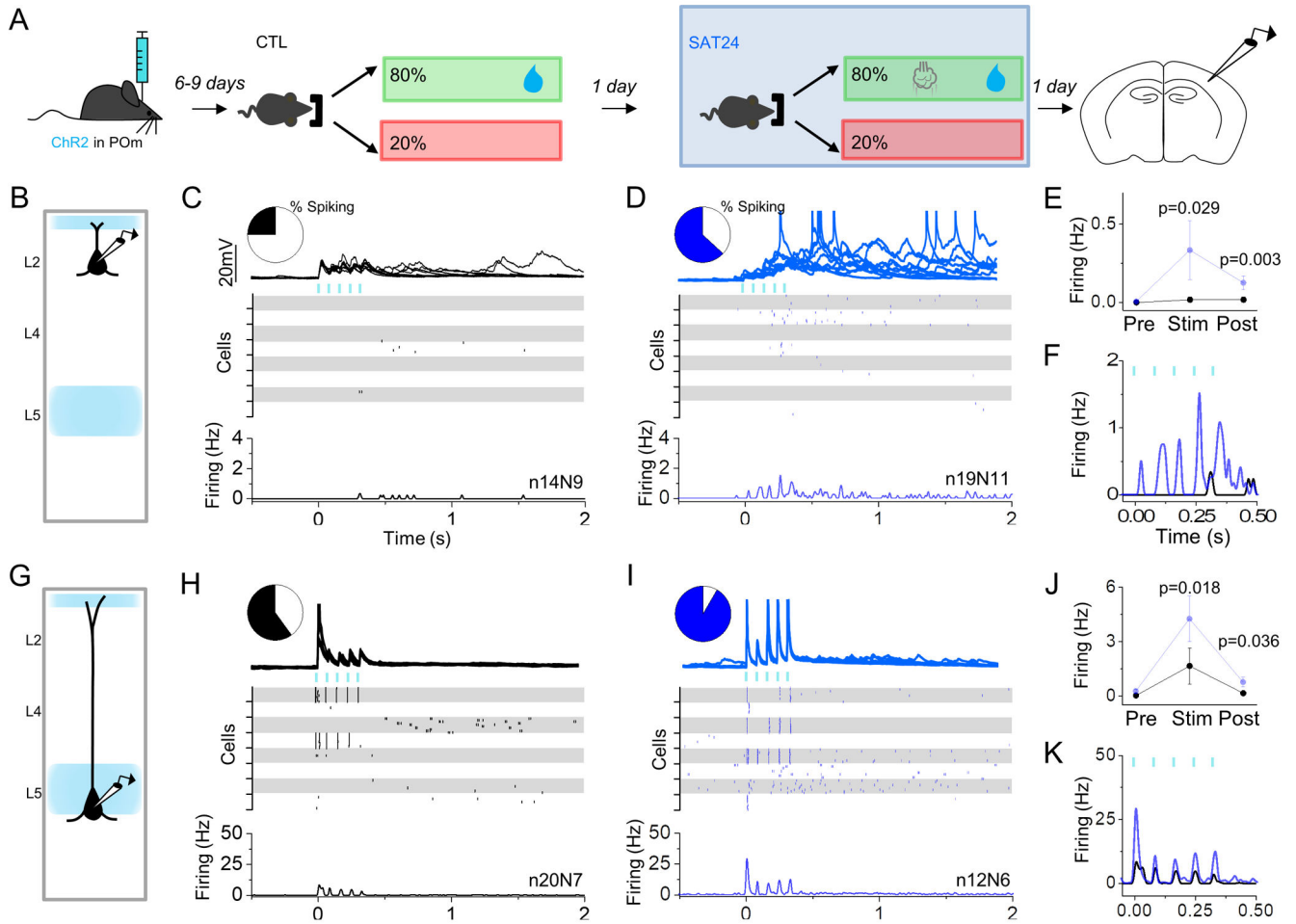


Figure 2. Increase in POM-evoked cortical activity after 24 hrs of SAT.

(A) Schematic of experiment with recordings performed in Chr2-injected mice after 24 hrs of acclimation and 24 hrs of SAT. (B) Schematic of POM axonal labeling and laminar pyramidal neuron recording site in L2. (C,D) POM-evoked activity (blue bars, 5 pulses, 5ms, 80 ms ISI) in L2 Pyr neurons of control animals that received 24 hrs of acclimation (left, black) and 24 hrs SAT (blue, right). Pie chart shows fraction of neurons that generated any action potentials following stimulation. Example cell response (top) shows 10 consecutive trials for an individual neuron. Raster (middle) shows spiking activity on 10 consecutive trials for 8 example cells. Global peri-stimulus time histogram (PSTH, bottom, 10ms bins) shows average firing frequency across all cells in group. (E) Average firing frequency across all cells during the 500ms preceding POM stimulation (Pre), during stimulation (Stim) and directly following stimulation (Post). (F) Overlay of POM-evoked spiking activity (10ms bins) for CTL (black) and SAT24 (blue) animals. (G-K) Same as C-F, but for L5 Pyr neurons. Averages represented as mean \pm SEM. See also Figure S1.

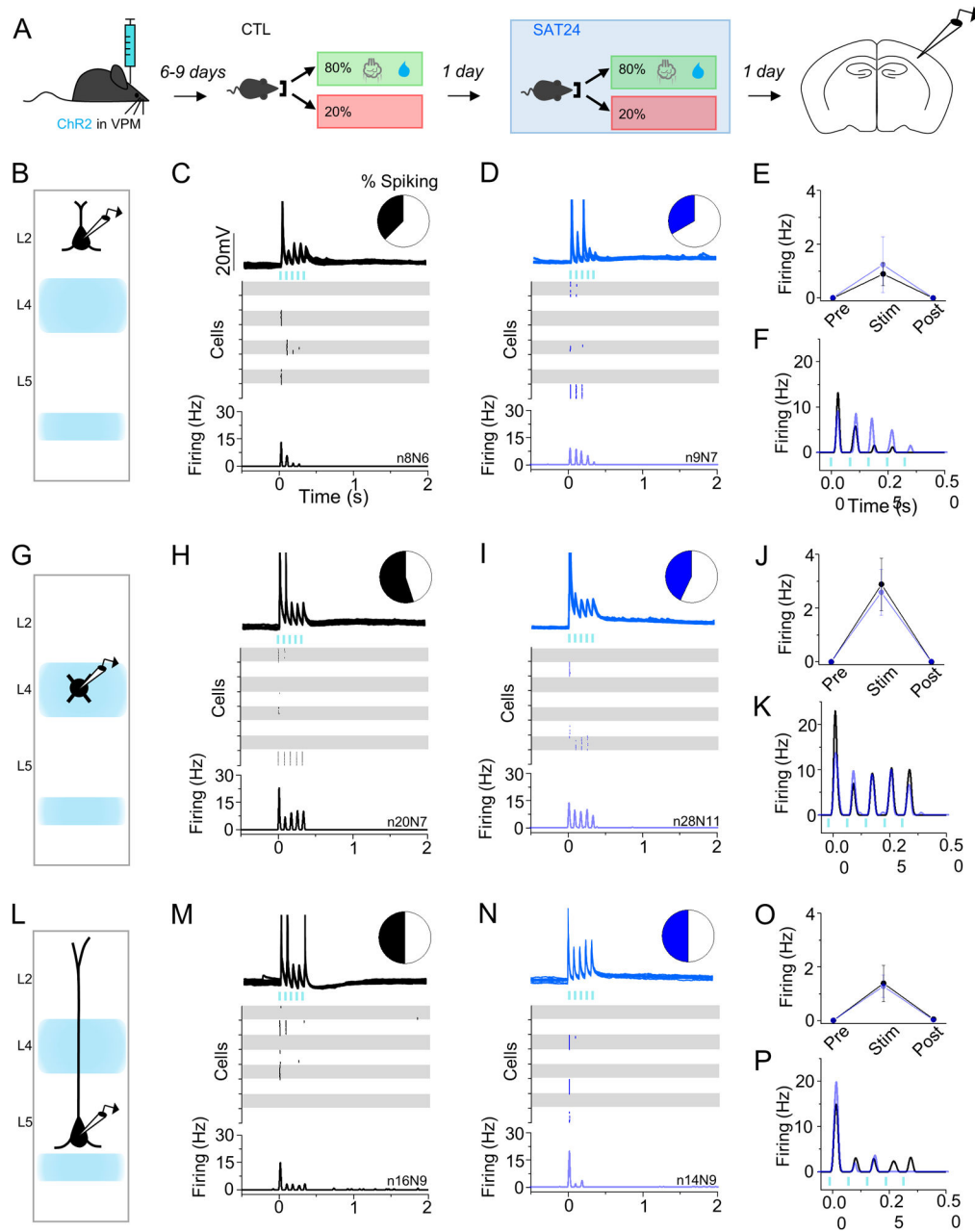


Figure 3. No change in VPM-evoked cortical activity after 24 hrs of SAT.

(A) Schematic of experiment with recordings performed in ChrR2-injected mice after 24 hrs of acclimation and 24 hrs of SAT. (B) Schematic of VPM axonal labeling and laminar pyramidal neuron recording site in L2. (C,D) VPM-evoked activity (blue bars, 5 pulses, 5ms, 80 ms ISI) in L2 Pyr neurons of control animals that received 24 hrs of acclimation (left, black) and 24 hrs SAT (blue, right). Pie chart shows fraction of neurons that generated any action potentials following stimulation. Example cell response (top) shows 10 consecutive trials for an individual neuron. Raster (middle) shows spiking activity on 10 consecutive trials for 8 example cells. Global PSTH (bottom, 10ms bins) shows average firing frequency across all cells in a population. (E) Average firing frequency across all cells during the

500ms preceding VPM stimulation (Pre), during stimulation (Stim) and directly following stimulation (Post). (F) Overlay of VPM-evoked spiking activity for CTL (black) and SAT24 (blue) animals. (G-K) Same as C-F, but for L4 excitatory neurons. (L-P) Same as C-F but for L5 Pyr neurons. Averages represented as mean \pm SEM. See also Figure S2.

Author Manuscript

Author Manuscript

Author Manuscript

Author Manuscript

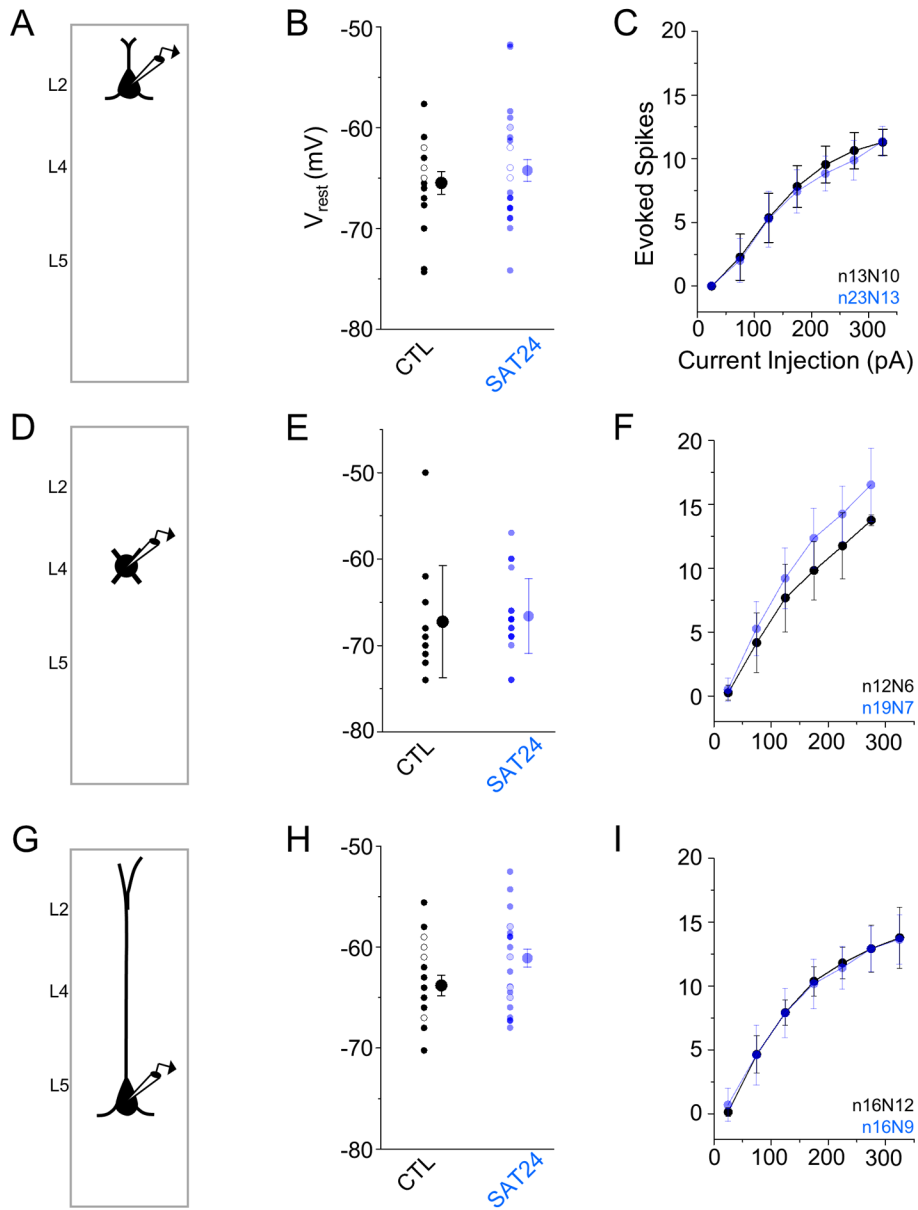


Figure 4. No change in intrinsic properties of cortical excitatory neurons after SAT.

(A) Schematic of experimental setup. (B) Average resting membrane potential of L2 Pyr neurons from CTL (black) and SAT24 (blue) animals. Open circles indicate cells recorded in the presence of the synaptic blockers picrotoxin (50uM), APV (50uM), and NBQX (25uM) and are included in the displayed average. (C) Average spike count during 500ms current injections (25pA steps) for L2 Pyr neurons from CTL (black) and SAT24 (blue) animals. Displayed values include a subset of cells recorded in the presence of synaptic blockers described in (B). (D-F) Same as (A-C) but for L4 excitatory neurons. (G-I) Same as (A-C) but for L5 Pyr neurons. Averages represented as mean \pm SEM.

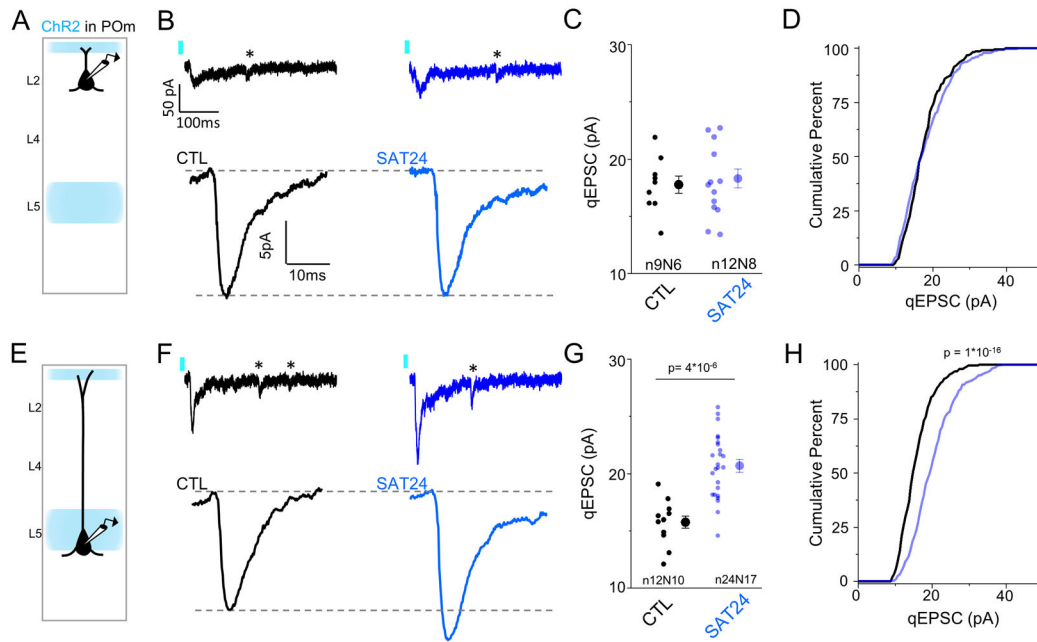


Figure 5. 24 hrs of SAT strengthens POM synaptic inputs onto L5 Pyr neurons.

(A) Schematic of experimental setup in L2 Pyr neurons. (B) Top: Example single trial showing Sr^{2+} -desynchronized POM-evoked response in a L2 Pyr neuron where individual, isolated quantal events (*) follow an initial multiquantal response. Bottom: Global average qEPSCs from control animals (black, left) or in animals that received 24 hrs of SAT (blue, right). All well-isolated light-evoked qEPSCs in a cell (25 for inclusion) were aligned to rise time and averaged to generate an average cellular POM qEPSC. Cell averages were aligned to rise and averaged to generate global average qEPSC for each condition. (C) Quantification of mean qEPSC amplitude for each cell, measured as the mean of individual qEPSC peak amplitudes within a cell. (D) Cumulative distribution histogram of POM qEPSC amplitudes for CTL (black) and SAT24 (blue) animals. Distributions comprise 25 randomly selected events from each cell, compared using a K-S test. (E-H) Same as (A-D) but for L5 Pyr neurons. Averages represented as mean \pm SEM. See also Figure S3.

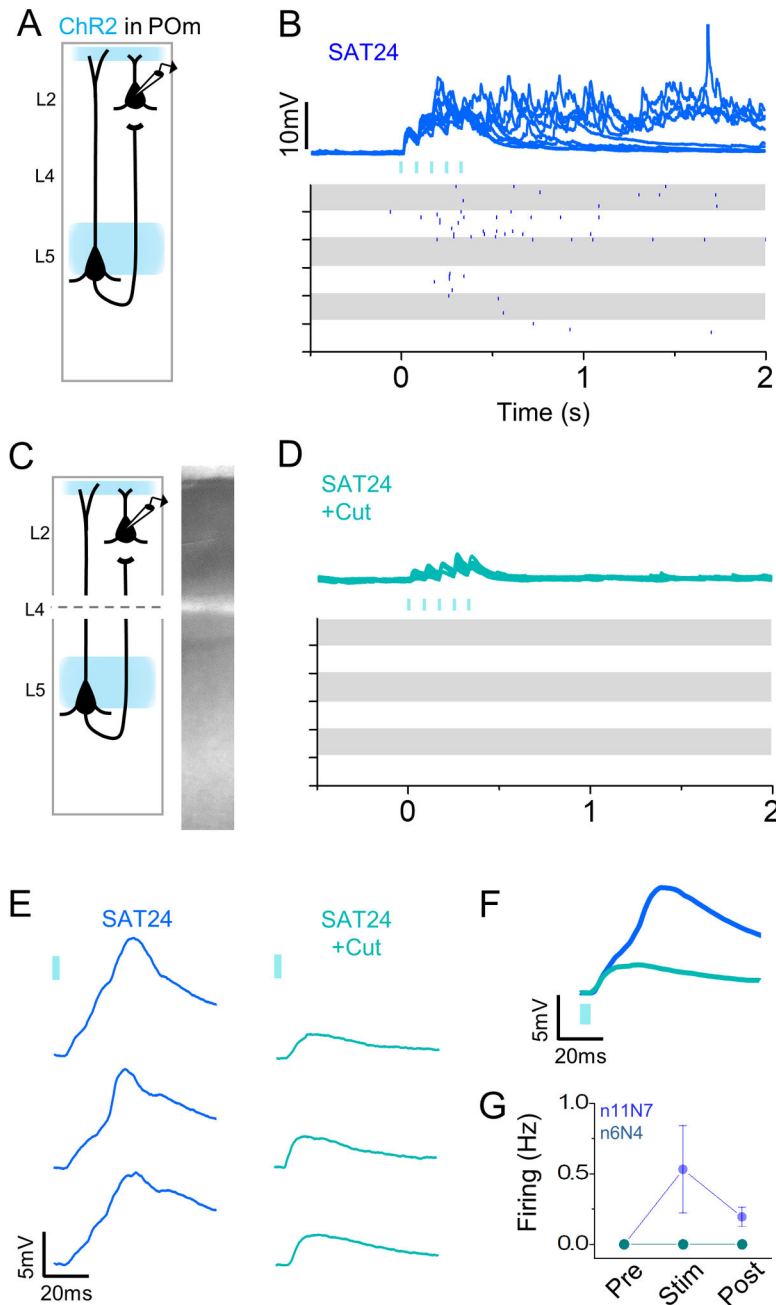


Figure 6. Elevated POM-evoked activity in trained animals is driven by ascending input from infragranular layers.

(A) Schematic of experimental setup for ChR2-evoked firing of Pre-Cut L2 Pyr neurons in SAT24 animals. (B) Light-evoked activity (blue bars, 5 pulses, 5m, 80ms ISI) on 10 consecutive trials in an example L2Pyr cell (top) and for 10 example cells (bottom) in SAT24 animals. (C-D) Same as (A-B) but for L2 Pyr neurons after a mechanical incision through cortical L4. Each collected post-cut cell had at least one recorded L2 Pyr recording in the same slice prior to cut, and example cells in (B,D) were recorded in the same slice. (E) Comparison of subthreshold responses on 3 consecutive sweeps following the first light

pulse for example cells in (B,D). (F) Average response (10 consecutive sweeps) to first light pulse for SAT24 (dark blue), and SAT24+Cut (light blue) example cells in (B,D). (G) Average firing frequency across all cells during the 500ms preceding VPM stimulation (Pre), during stimulation (Stim) and directly following stimulation (Post). Averages represented as mean \pm SEM. See also Figure S4.

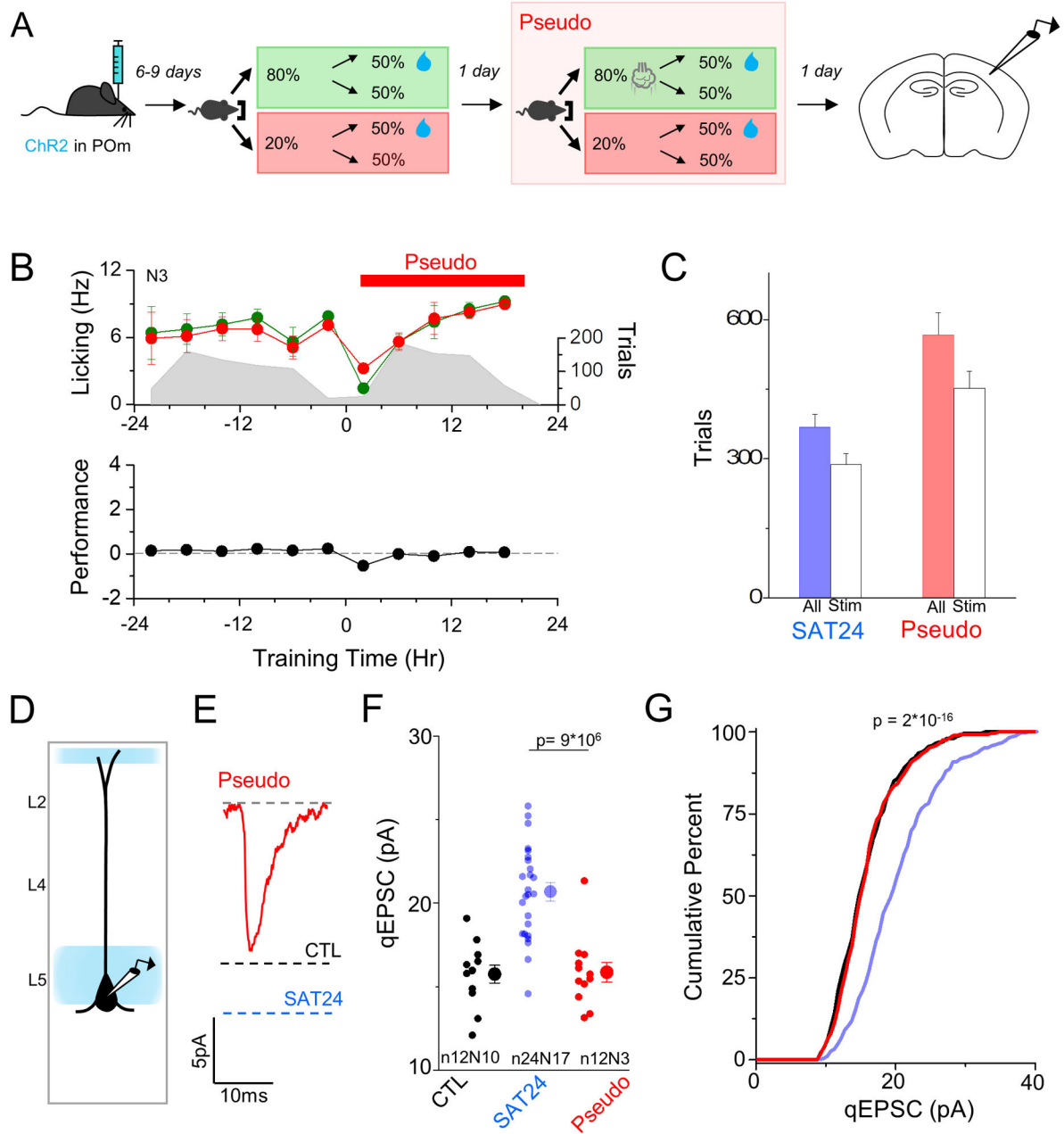


Figure 7. Sensory stimulation alone does not drive POM plasticity.

(A) Schematic of experimental setup and pseudo-training behavioral paradigm. Cages, training structure, stimulus, and timing were identical to SAT but water delivery (US) was uncoupled from (CS) and randomly delivered on 50% of trials regardless of CS presentation. (B) Time course of anticipatory lick rates (left axis, 300ms prior to water delivery, 4 hr bins) over the course of training for blank (20%, red) and stim trials (80%, green) averaged across all animals. Trial initiation counts (right axis) are shown in grey for the same time bins, red bar denotes pseudo-training period. (C) Comparison of animal-initiated trial counts during 24 hrs of SAT (blue) and Pseudotrained (red). Solid bars indicate total trials received while white bars show the number of stimulus (CS) trials received. (D) Schematic of experimental

setup. (E) Global average qEPSC in Pseudotrained animals. All well-isolated light-evoked qEPSCs in a cell (25) were aligned to rise time and averaged to generate an average cellular POM qEPSC. Cell averages were aligned to rise and averaged to generate global average qEPSC. Global average POM qEPSC amplitudes in control (black) and SAT24 (blue) animals for comparison. (F) Quantification of average qEPSC amplitude for each cell, measured as the average of individual qEPSC peak amplitudes within a cell. CTL and SAT24 replotted from Fig. 4 (G) Cumulative distribution histogram of POM qEPSC amplitudes for CTL (black) and SAT24 (blue) animals and Pseudo-trained animals (red). Distributions comprise 25 randomly selected events from each cell and stats are for a K-S test between 24 hr and pseudo. Averages represented as mean \pm SEM. See also Figure S5.

Author Manuscript

Author Manuscript

Author Manuscript

Author Manuscript

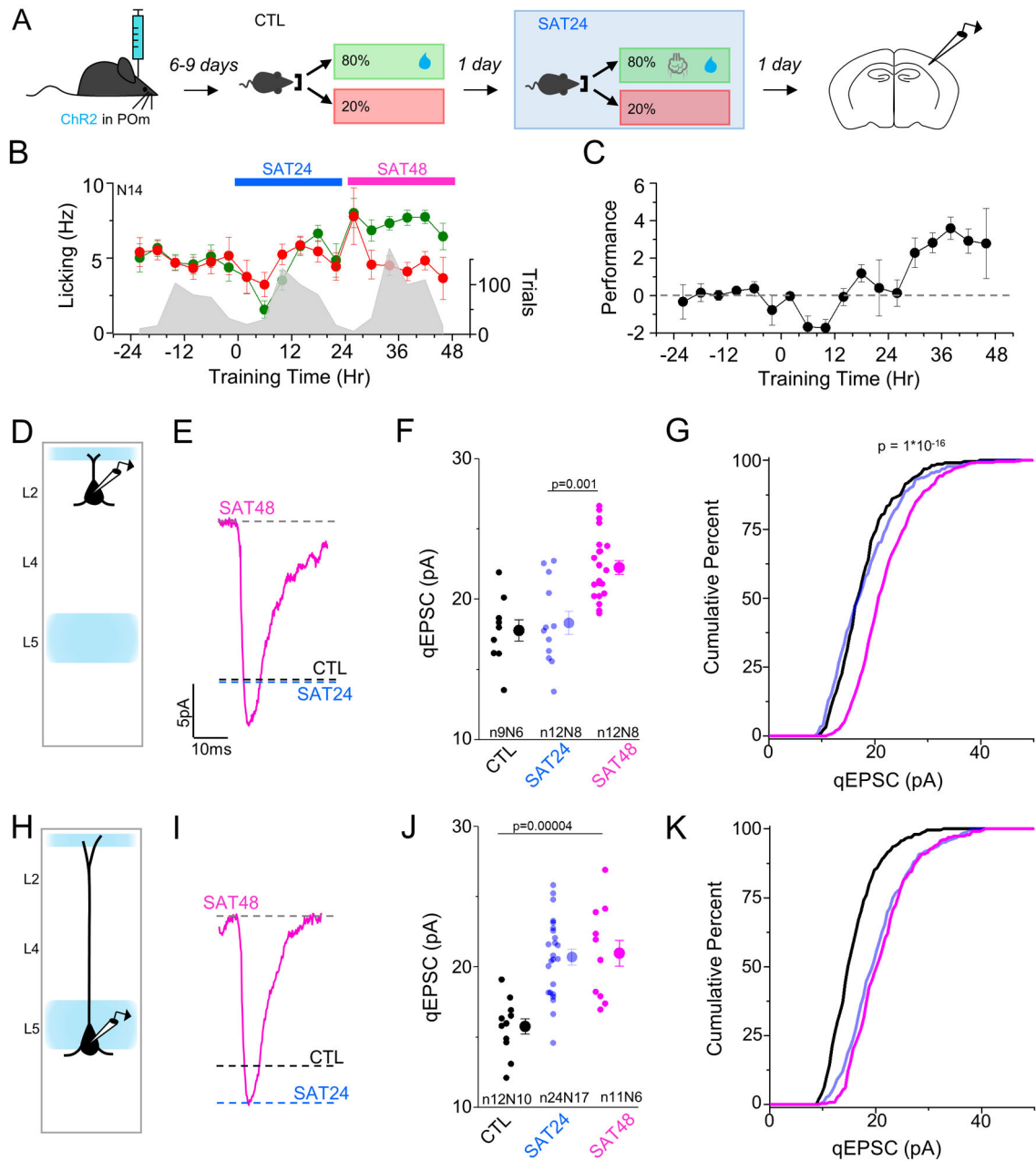


Figure 8. SAT drives sequential thalamocortical plasticity in L5 then L2 Pyramidal neurons. (A) Schematic of experiment with recordings performed in Chr2-injected mice after 24 hrs of acclimation and 48 hrs of SAT. (B) Time course of anticipatory lick frequency (left axis, 300ms prior to water delivery, 4 hr bins) over the course of acclimation and training for blank (red) and stim/water trials (green) averaged across all animals (N=14 for all timepoints). Trial initiation counts (right axis) are shown in grey for the same time bins. (C) Quantification of performance defined as the difference in anticipatory lick rates between stim/water trials and blank trials during learning for the 4 hour bins shown in (B). (D) Schematic of experimental setup for recording POm qEPSCs in L2 Pyr neurons. (E) Global average qEPSC in SAT48 animals. All well-isolated light-evoked qEPSCs in

a cell (25) were aligned to rise time and averaged to generate an average cellular POM qEPSC. Cell averages were aligned to rise and averaged to generate global average qEPSC. Global average POM qEPSC amplitudes in control (black) and SAT24 (blue) animals for comparison (F) Quantification of average qEPSC amplitude for each cell, measured as the average of individual qEPSC peak amplitudes within a cell for control (black), SAT24 (blue), and SAT48 (magenta) animals. (G) Cumulative distribution histogram of POM qEPSC amplitudes for CTL (black) and SAT24 (blue) animals and SAT48 animals (magenta). Distributions comprise 25 randomly selected events from each cell, K-S test compares Pseudo and 24 hrs. (H-K) Same as D-G but for L5 Pyr neurons. Averages represented as mean \pm SEM. See also Figure S6.

Author Manuscript

Author Manuscript

Author Manuscript

Author Manuscript

Key Resources Table

REAGENT or RESOURCE	SOURCE	IDENTIFIER
Bacterial and Virus Strains		
AAV1.CAG.hChR2(H134R)-mCherry.WPRE.SV40	Addgene	Cat#100054-AAV1
AAV2-hSyn-hChR2(H134R)-EYFP	UNC Vector Core, Deisseroth Lab	
Chemicals, Peptides, and Recombinant Proteins		
Tamoxifen	Tocris	Cat# 6342
Ketoprofen	Sigma-Aldrich	Cat# K1751
QX-314 (N-ethyl bromide)	Tocris	Cat# 2313
AP5	Tocris	Cat# 0106
Picrotoxin	Tocris	Cat# 1128
Experimental Models: Organisms/Strains		
C57Bl6 Mice (Harlan)	Jackson Laboratory	Cat# 000664
Nelf1Cre Mice	MMRC	Cat# 037424-UCD
ETV1creER Mice	Jackson Laboratory	Cat# 012048
Ai32 Mice	Jackson Laboratory	Cat# 024109
Software and Algorithms		
Igor Pro 6.0	Wavemetrics	
Minianalysis	Synaptosoft	
Other		
Custom Injection Cannulas	Plastics One	
IR Beam Break Sensor	Adafruit	Cat#2167
Yun Shield v2.4	Dragino	
Leonardo	Arduino	Cat# A000057
WifiShield 2.4	Df Robot	Cat# TEL0047
Solenoid Valve	The Lee Company	Cat# LHDA1233115H
Capacitive touch sensor AT42QT1010	Adafruit	Cat#1374
White LED (Version)	Prizmatix	UHP-T-LED-White-High-CRI
Bipolar Stimulating Electrode	FHC	Cat# CBCRC75